AN ABSTRACT OF THE THESIS OF

MIROSLAV GREGORIČ for the degree of MASTER OF SCIENCE

in MECHANICAL ENGINEERING presented on AUGUST 4, 1978

Title: AN EXPERIMENTAL INVESTIGATION OF MERGING BUOYANT JETS IN A CROSSFLOW

Abstract approved: Redacted for Privacy

Lorin R. Davis

Merging isothermal buoyant jets in a crossflow were investigated experimentally. Jets of salt water were discharged from a constant head tank into the stagnant tap water. A crossflow was simulated by towing the discharge ports through the receiving water at desired speeds. Visualization of the jet cross-sections produced by a vertical slit light source and fluorescein dye was recorded as a sequence of pictures taken by a motor-driven camera. Maximum heights, widths, and vertical cross-sections of deflected buoyant jets for different velocity ratios, number of nozzles and nozzle line orientation were plotted against downstream location.

Horseshoe shaped cross section was observed and recorded in the case of single jet in crossflow and multiple jet crossflow parallel to nozzle line, while in the case of crossflow perpendicular to nozzle line horseshoe pattern was not clear. Wake behind the multiple jets in crossflow was observed and recorded, with distinct vortex street behind.

Experimental results show that single jets dilute more rapidly so the cross-sections are larger and trajectories lower.

Increasing velocity ratio for fixed N and θ_1 lowers the trajectories and reduces plume widths and normalized cross-sectional area; all of them appear to increase linearly with x (from x=10 D on).

Increasing number of ports for fixed R and θ_1 raises the trajectories and reduces normalized cross-sectional areas rapidly.

Changing the angle θ_1 between crossflow and line connecting the ports for fixed R and N strongly influences cross-sections. At $\theta_1 = 0^o$ vortex pair is dominant and normalized areas are the largest. At $\theta_1 = 45^o$ jets are rolled in space like a band and vortex pair can be seen. At 90^o vortex appears only at the lowest velocity ratio R = 0.1.

Experimental Investigation of Merging Buoyant Jets in a Crossflow

by

Miroslav Gregorič

A THESIS

submitted to

Oregon State University

in partial fulfillment of
the requirements for the
degree of

Master of Science

Completed August 1978

Commencement June 1979

APPROVED:

Redacted for Privacy

Professor of Department of Mechanical Engineering
in charge of major

Redacted for Privacy

Head of Department of Mechanical Engineering

Redacted for Privacy

Dean of Graduate School

Date thesis is presented August 4, 1978

Typed by CAMPUS PRINTING & COPY CENTER for MIROSLAV GREGORIČ

ACKNOWLEDGEMENT

I wish to express my personel indebtedness to the Department of Mechanical Engineering and in particular to Dr. James R. Welty, Head of the Department, for accepting me for graduate studies, and my major professor, Dr. Lorin R. Davis for giving me the opportunity to work in the field of this investigation. Furthermore, I would like to acknowledge the assistance of the Corvallis Environmental Protection Agency Laboratory, more specifically to Dr. M. A. Shirazi for granting me the use of their Hydraulics Laboratory.

Also my greatest appreciation is extended to Dr. Larry D. Winiarski, Dr. Walter E. Frick, and Robert B. Macduff, for interest, valuable discussions and suggestions for the duration of this research.

I also want to recognize the support of Institute Jozef Stefan, Ljubljana, Yugoslavia, who gave me leave for the period of my studies and International Atomic Energy Agency, Vienna, Austria, who supported my stay at Oregon State University.

Special thanks to Allen George and Sherry Smith who helped me with the manuscript.

There are no proper words to express my gratidude to my wife Katja and son Žiga for their patience and continued tolerance of my long absence.

Additional thanks go to all those not mentioned here who aided me along the way.

TABLE OF CONTENTS

LIST OF ILLUSTRATIONS

LIST OF PLATES

LIST OF TABLES

LIST OF SYMBOLS

N	Number of discharge ports
A_x	Area of jet(s) cross-section perpendicular to x-axis.
D_o	Port discharge diameter
F_o	Densimetric Froude number at outlet, $U_o/(g'D_o)^{\frac{1}{2}}$
g	Acceleration due to gravity
g'	Reduced gravitational acceleration, $g \frac{\Delta\rho}{\rho_a}$
L	Distance between ports
R	Velocity ratio = U_∞/U_o
S	Salinity of the jet
T_a	Ambient temp (in the channel)
T_o	Jet discharge temperature
t	Time
U_o	Discharge velocity
U_∞	Crossflow velocity (ambient, towing)
X	Rectilinear horizontal coordinate, downstream
Y	Rectilinear horizontal coordinate
Z	Reclilinear vertical coordinate (pointed down in channel)
ρ_a	Density of ambient water (in the channel)
ρ_o	Density of discharging water
Δ_ρ	Density difference = $\rho_o - \rho_a$
θ_1	Angle between crossflow and port connection line
ν	Kinematic viscosity

SUBSCRIPTS

a	Ambient
o	Discharge

I. INTRODUCTION

Jets have been the subject of investigation for many years and whole textbooks have been written on this subject (1,2,3). Jets can be laminar or turbulent, two dimensional, axis-symetric or three-dimensional. They can be momentum or buoyant and they can discharge into steady or flowing environment, which can be stratified in addition. These jets appear alone or in groups. One can further challenge the investigators by spicing the problem with the addition of moisture effects for stacks and cooling tower plumes or effects of free surface in shallow water and transient phenomena in tidal regions.

A concise state-of-the-art review of thermal plume modeling techniques is presented in (4). Excellent reviews are also in (5) and (6). Multiport jets were studied in (7,8,9). Experimental data are rare. Multiport buoyant discharge into crossflow was investigated experimentally in (10), simulating infinite line of ports. Data for finite number of ports for buoyant discharge with no ambient current are reported in (11). No similar data exist for crossflow. In this investigation an effort was made to get some characteristics of a group of buoyant jets discharging perpendicularly from single ports placed in a row into uniform crossflow. Influence of number of discharge ports and direction of the crossflow was also studied. Such merging buoyant jets have application in power generation waste heat disposal into environment. This could be river or ocean and the ports would be called multiport diffusers or could be just a breeze over

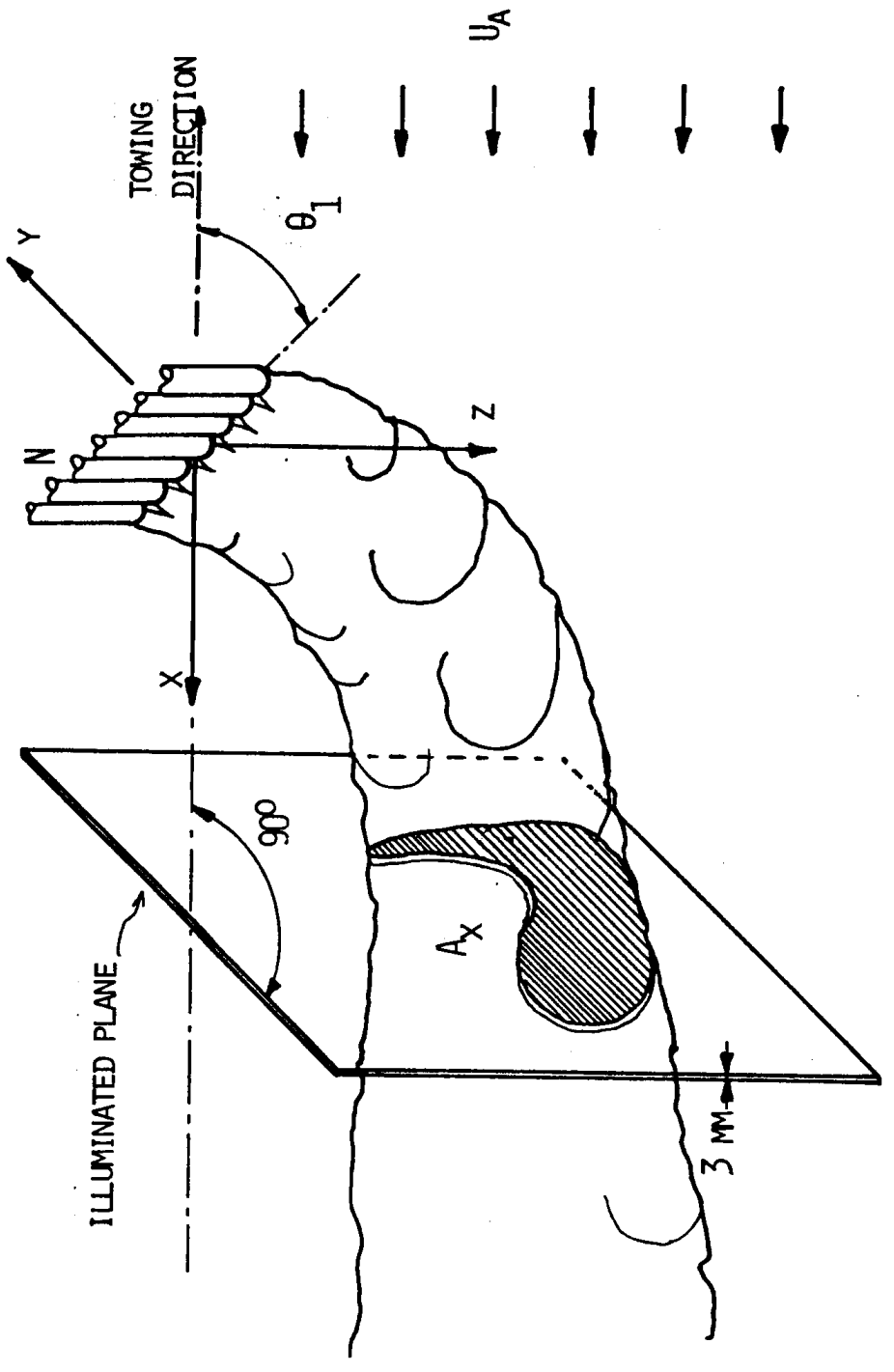

FIGURE 1: Definition sketch of merging buoyant jets in a crossflow.

the country and the ports would be called multiple cell cooling towers. This investigation idealized the real process as much as possible and the only goal was to get some data which could be later used to check or tune computer models. Visualization method which was used in this investigation is somewhat rare in this field. It gave the three dimensional picture of the merging buoyant jets in a crossflow.

All experimenters know that once a phenomenon is visualized it is much easier to understand it and to apply the proper mathematical model to obtain theoretical solutions. Flow visualization techniques are numerous and they are being used in some form in all laboratories dealing with fluid flow. They are applied for gas and liquid flows at all velocities. Sometimes it is possible to understand the entire development of the flow from one observation. Such techniques are very elegant, but sometimes need considerable experience to interpret. A quantitative evaluation of obtained flow pictures is laborious.

Flows in water can be visualized by introducing solid tracers (e.g. aluminum particles, polystyrene beads, glass beads, tellurium particles emitted by a cathode upstream from the test solution). The particles, if small enough will follow the path of the fluid for a while even if the particle density is not the same as the fluid density. Liquid tracers are most often used for the marking of filament lines. Different dyes are used: food coloring, writing ink, gentian violet, methylene blue dye, fluorescent rhodamine,

fluorescein and many others. Milk (sometimes mixed with dyes, water or alcohol) was found excellent for marking filament lines. It makes the line contrast greatly with the fluid and has lower diffusion than other tracers.

The disadvantage of these dye methods is that they are not suited for use in a closed-circuit water tunnel, since the dye recirculates and contaminates the water. Only short time observation can be made. A similar situation occurs in a towing channel. The system has to be emptied and refilled after each experiment.

Gaseous tracers injected in the flow or formed naturally during the experiment (for example by cavitation) or formed by electrolysis (for example hydrogen bubbles) can be used in many experiments.

Once the flow field is marked with visible tracers one can record the picture on photographic film. If the flow is two-dimensional it is easy to obtain good pictures. To get three-dimensional resolution one should illuminate a thin plane slice of the flow field, so that only the light scattered from the tracer within this illuminated sheet can reach the camera. This method was used in the present investigation.

Optical methods for compressible flows need no additional tracer to mark the flow. These methods are based on optical disturbances caused by the nonhomogeneity of flow field with respect to light path. Most known methods are shadowgraph, Schlieren and interferometer. Optical arrangements could be very sophisticated.

Excellent reviews of different visualization techniques for use in gases and liquids can be found in (12, 13), and in (14, 15) for use in water only. Reference (16) gives abstracts of numerous applications of these techniques.

Development of modeling parameters is presented in Chapter 2 with detailed description of experimental apparatus and visualization technique in Chapter 3. Results are discussed in Chapter 4 and a brief summary of the work follows in Chapter 5.

II. MODELING PARAMETERS FOR MERGING BUOYANT JETS IN A CROSSFLOW

The analysis in this chapter considers finite array of round turbulent buoyant jets discharged vertically to a horizontal crossflow (with uniform velocity and density) from arbitrary directions. (Fig. 1)

List of all variables that describe this flow:

Variable	Symbol	Dimension	
position (along crossflow)	x	L	
jet diameter	D_o	L	
exit velocity	U_o	Lt^{-1}	Round Momentum Jet
fluid viscosity	μ	$ML^{-1}t^{-1}$	
jet density	ρ_o	ML^{-3}	
ambient density	ρ_a	ML^{-3}	
excess density	$\rho_o-\rho_a$	ML^{-3}	Buoyant
gravitational acceleration	g	Lt^{-2}	
ambient characteristic length	L_a	L	
ambient velocity	U_a	Lt^{-2}	Uniform Crossflow
number of ports	N		
spacing between ports	L	L	Finite Array Of Merging Jets
angle between the line connecting the ports and crossflow	θ_1		

The variables have units of length, time and mass only, so according to Buckingham Π-theory there will be ten dimensionless groups.

$\Pi_1 = U_o^a D_o^b \rho_o^c x$		Round Momentum Jet
$\Pi_2 = U_o^a D_o^b \rho_o^c \mu$		
$\Pi_3 = U_o^a D_o^b \rho_o^c \rho_a$		
$\Pi_4 = U_o^a D_o^b \rho_o^c (\rho_o - \rho_a)$		Buoyant
$\Pi_5 = U_o^a D_o^b \rho_o^c g$		
$\Pi_6 = U_o^a D_o^b \rho_o^c L_a$		Uniform Crossflow
$\Pi_7 = U_o^a D_o^b \rho_o^c U_a$		
$\Pi_8 = U_o^a D_o^b \rho_o^c N$		
$\Pi_9 = U_o^a D_o^b \rho_o^c L$		Merging
$\Pi_{10} = U_o^a D_o^b \rho_o^c \theta_1$		Orientation

Exponents a, b and c must be determined so that in each group Π becomes dimensionless.

Result is:

Dimensionless length $\Pi_1 = \frac{x}{D_o}$

Reynolds number

$$\Pi_2 = \frac{\mu}{U_o D_o \rho_o} = \frac{1}{R_e} = \frac{\nu}{U_o D_o} = \frac{U_1/D_o^2}{U_o^2/D_o} = \frac{\text{viscous force}}{\text{inertial force}}$$

Density ratio:

$$\Pi_3 = \frac{\rho_a}{\rho_o}$$

Density deficiency:

$$\Pi_4 = \frac{\rho_o - \rho_a}{\rho o} = \frac{g\,(\rho_o - \rho_a)/\rho_o}{g} = \frac{\text{buoyancy force}}{\text{gravity force}}$$

Froude number:

$$\Pi_5 = \frac{D_o g}{U_o^2} = \frac{1}{Fr} = \frac{g}{U_o^2/D_o} = \frac{\text{gravity force}}{\text{inertial force}}$$

Ambient length

$$\Pi_6 = \frac{L_a}{D_o}$$

Velocity Ratio

$$\Pi_7 = \frac{U_a}{U_o}$$

Number of ports:

$$\Pi_8 = N$$

Port spacing:

$$\Pi_9 = \frac{L}{D_o}$$

Angle

$$\Pi_{10} = \theta_1 \quad .$$

Combining Π_5, Π_4 and Π_3 one can get:

$$\frac{\Pi_3}{\Pi_5\,\Pi_4} = \frac{\rho_a/\rho_o}{(D_o g/U_o^2)\;(\rho_o - \rho_a)/\rho} =$$

$$= \frac{U_o^2}{\frac{\rho_o - \rho_a}{\rho_a}\,g\,D_o} = \frac{U_o^2/D_o}{\frac{\rho_o - \rho_a}{\rho_a}\,g} = \frac{\text{inertia force}}{\text{buoyancy force}}$$

Square root of this is known as densimetric source Froude number

$$\left(\frac{\Pi_3}{\Pi_5\ \Pi_4}\right)^{0.5} = \frac{U_o}{\sqrt{\frac{\rho_o - \rho_a}{\rho_a} g\, D_o}} = \frac{U_o}{\sqrt{g\, D_o}} = F_o$$

Combining Π_2, Π_3, Π_6 and Π_7 one can get ambient Reynolds number:

$$\frac{\Pi_2\ \Pi_3}{\Pi_6\ \Pi_7} = \frac{\mu}{U_o D_o \rho_o} \frac{\rho_o}{\rho_a} \frac{D_o}{L_a} \cdot \frac{U_o}{U_\infty} = \frac{\mu}{U_\infty L_a \rho_a} = \frac{1}{Re_a}$$

To limit the number of these parameters the following assumptions are made:

1. The jet flow is fully turbulent, so that $\Pi_4 = \frac{1}{Re}$ which includes fluid viscosity can be neglected.

2. Density differences between the jets and ambient fluid are small and important only in causing buoyant forces. So $\Pi_5 = \frac{\rho_a}{\rho_o}$ can be neglected.

3. The effect of ambient turbulence was not considered in this investigation. In natural systems the flow is expected to be fully turbulent, and hence the effect of differences in Reynolds numbers is negligible.

One should observe the Reynolds numbers when laboratory results are used to verify theoretical models. If the laboratory model is not functioning in the fully turbulent range, results may not be useful for application to field situations (17). However, the results of Fan (for normal discharge) (18) who compared the jets in a flume with

those in towing channels show little difference and he concluded that the effect of ambient turbulence can be neglected as a first approximation. Range of his experiments was $0 < x/D < 120$. So $\Pi_8 = \frac{L_a}{D_o}$ was not considered in this investigation.

4. The effect of (pure) Froude number $\Pi_5 = \frac{1}{Fr}$ was neglected.

The parameters which remain are:

downstream position x/D_o

densimetric Froude number $F_o = U_o/(g'D_o)^{\frac{1}{2}}$

velocity ratio $R = U_a/U_o$,

number of ports N, port spacing L/D_o,

and angle between the line connecting the ports and crossflow θ_1.

The dependent variables are

plume centerline coordinates, y/D_o and Z/D_o

horizontal plume width W

vertical plume width B

vertical cross-sectional area A_x

III. EXPERIMENTAL EQUIPMENT

3.1 Towing channel and discharge tank

The experiments were conducted at the Hydraulics Laboratory of the U.S. Environmental Protection Agency's Corvallis Environmental Research Laboratory.

The main tank was a towing channel 12.1 m long, 0.61 m wide and 0.91 m high (Figure 2). Both sides of the channel were made of 1.25 cm thick plexiglass. The bottom plate was 2.54 cm solid steel with built in heat exchanger over the whole area so that the bottom surface could be maintained at a constant high or low temperature by circulation of hot or chilled water supplied from connected heater or chiller via a network of pipes and regulators. In this way temperature stratification can be achieved. In these experiments this feature was not used. The whole channel could be tilted to level it with the water surface or maintain an inclined bottom surface.

The discharge tank on the ball bearing wheels was towed on the rails above the receiving channel by a steel wire cable and adjustable speed motor drive (Figure 3). The instrumentation cart was towed behind the discharge tank when measuring conductivity in the downstream portion of the plume. The discharge tank was airtight except for the breather tubes which maintained a constant level of ambient pressure so velocity head was constant regardless of the level in the tank. Buffles inside the reservoir served for dampening out the waves caused at each start of a tow.

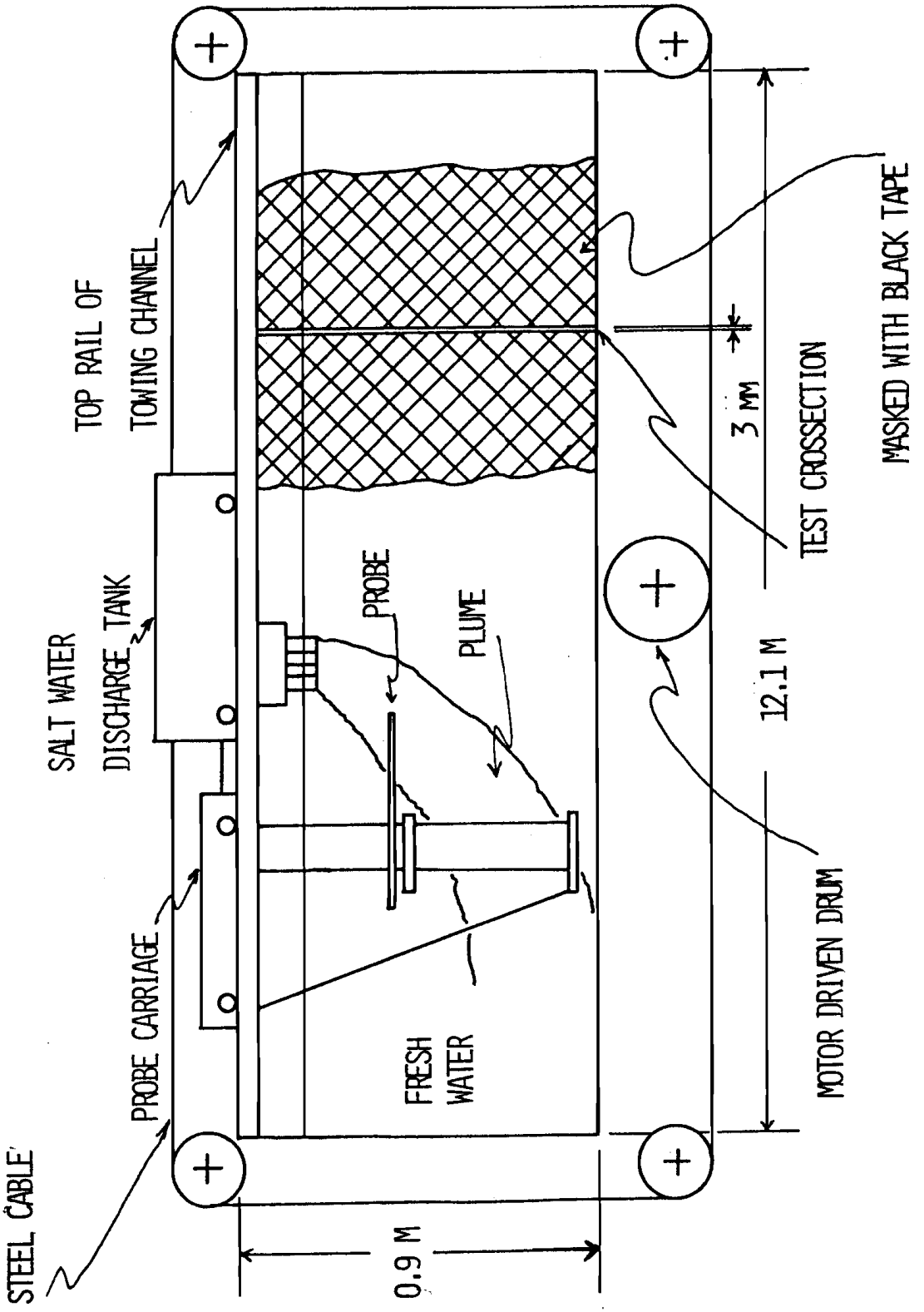

FIGURE 2: Towing Channel.

The tank with breather tubes was used in previous investigations [10]. From this tank the salt water passed through a control valve into a plenum chamber with buffer where it was evenly distributed to each of the discharge tubes. This arrangement was reported in [11]. Different discharge geometries could be attached to the plenum chamber. In this investigation only tubes, 9.53 mm inside diameter and 12.7 mm outside diameter were used. They were placed right against each other in a row. This yielded a port spacing to discharge diameter, L/D, of 1.33. The number of discharge ports used were 7, 5, 3, 2 and 1. The length of the tubes was sufficiently large to give fully developed turbulent flow at the discharge. Ports were oriented at 90, 45 and 0 degrees with respect to the direction of towing. Nominal Reynolds number for all runs was Re = 2500.

Salt water with salinity of 30 ppt was used in all experiments. It was prepared in a plastic barrel which was located above the level of the discharge tank (Figure 4). Six kg of salt (Morton salt for water softeners) was mixed with tap water to yield 0.2 m^3 of salt water. This volume was calibrated once, and the level marked on the wall. For each subsequent mixing tap water was added to the same level.

3.2 Photographic technique

On each side of the channel within the central part, the walls were masked with black tape to form a vertical slit 3 mm wide. The bottom of the channel in the vicinity of test cross-section was also blackened to prevent reflections. Light sources were placed on

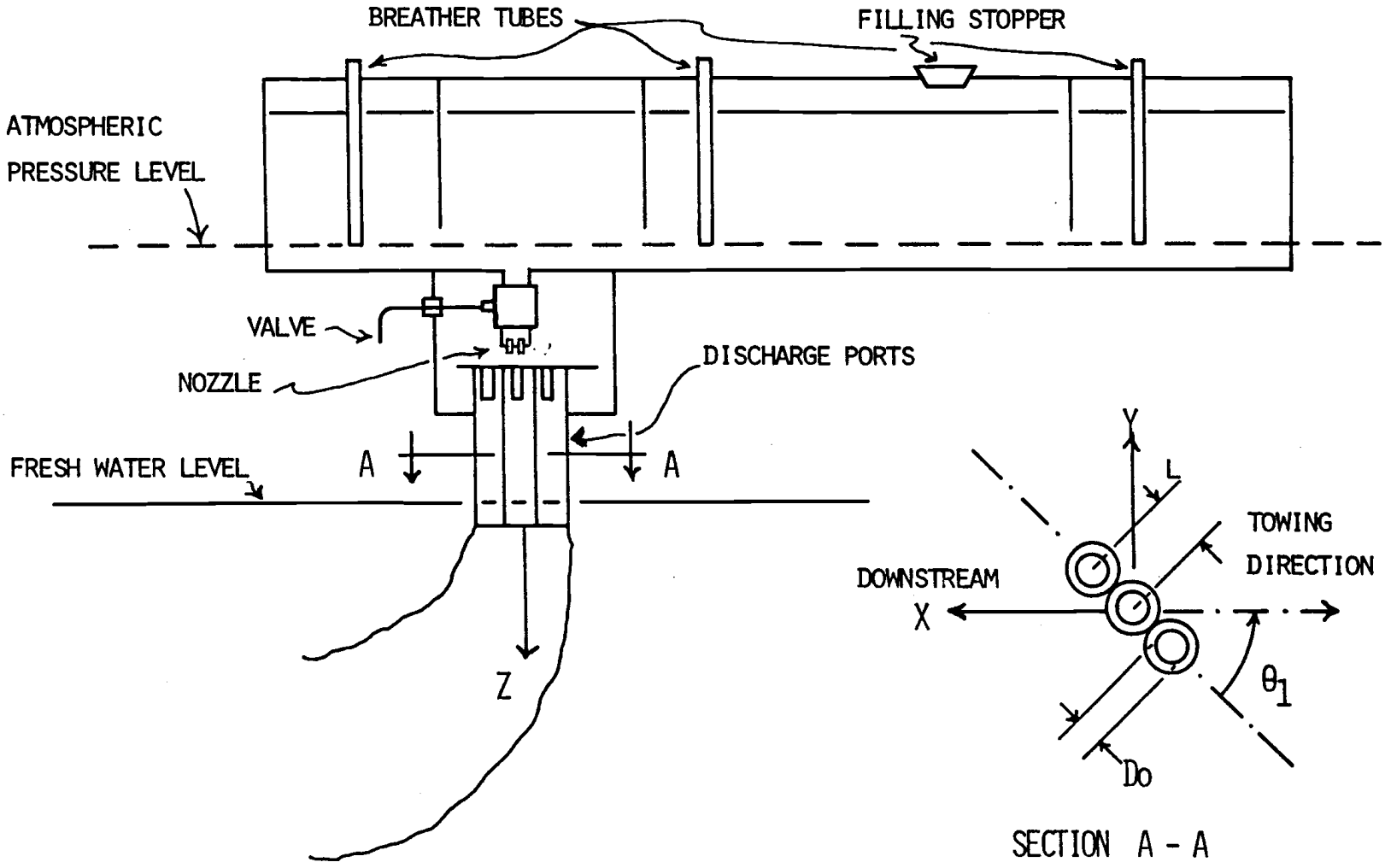

FIGURE 3: Discharge Tank.

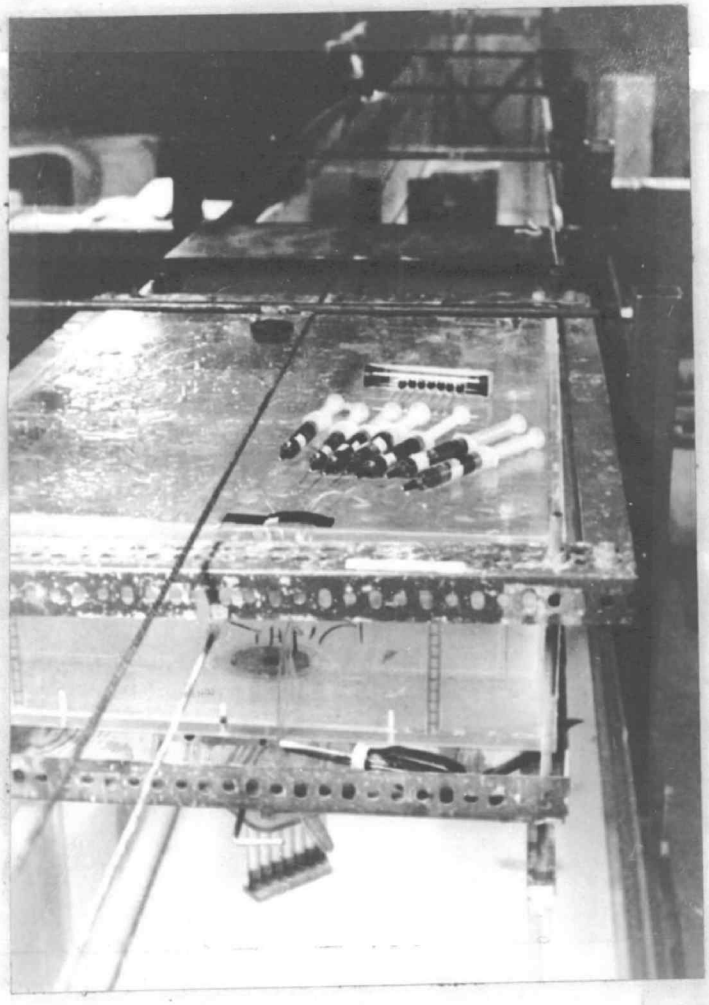

PLATE 1. Injection of Dye in the ports.

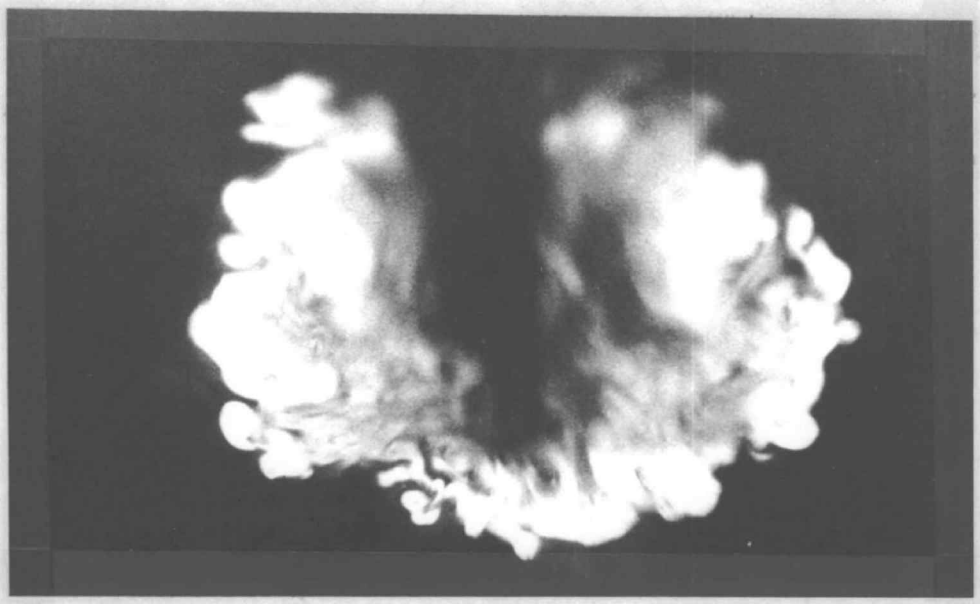

PLATE 2: Cross-sections thru the plane at $\theta_1 = 0$, N = 7, and R = 0.2.

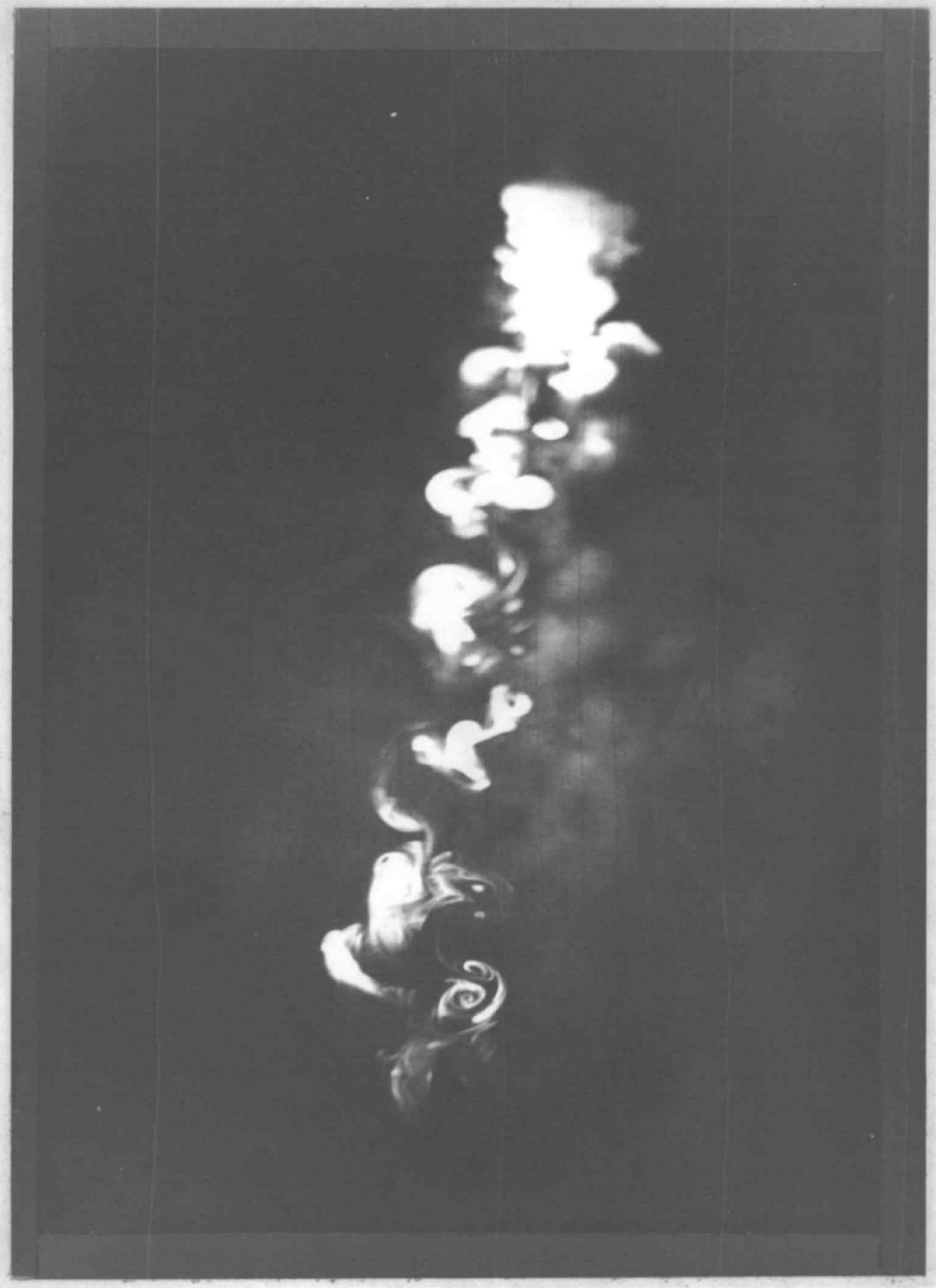

PLATE 3: Shedding behind the jets in a crossflow at $\theta_1 = 0$, N=7, and R=0.5.

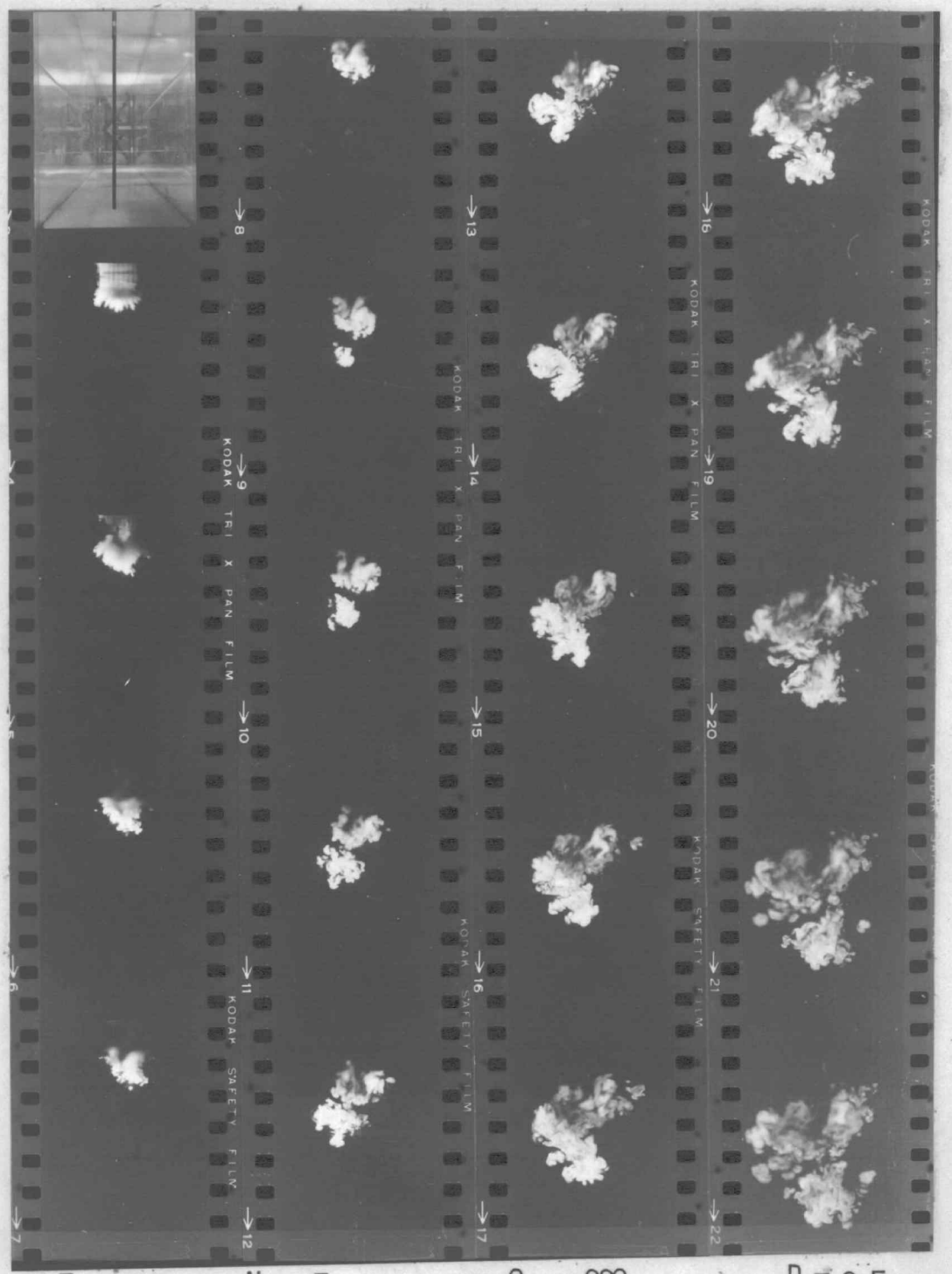

$F = 6.0$ $N = 7$ $\theta_1 = 90^0$ $R = 0.5$

$X_0 = 4.0$ $\Delta X/D_0 = 12.05$ EXPOSURE LENGTH = 3.6

PLATE 4 ; Cross-sections through buoyant jet for Run 111

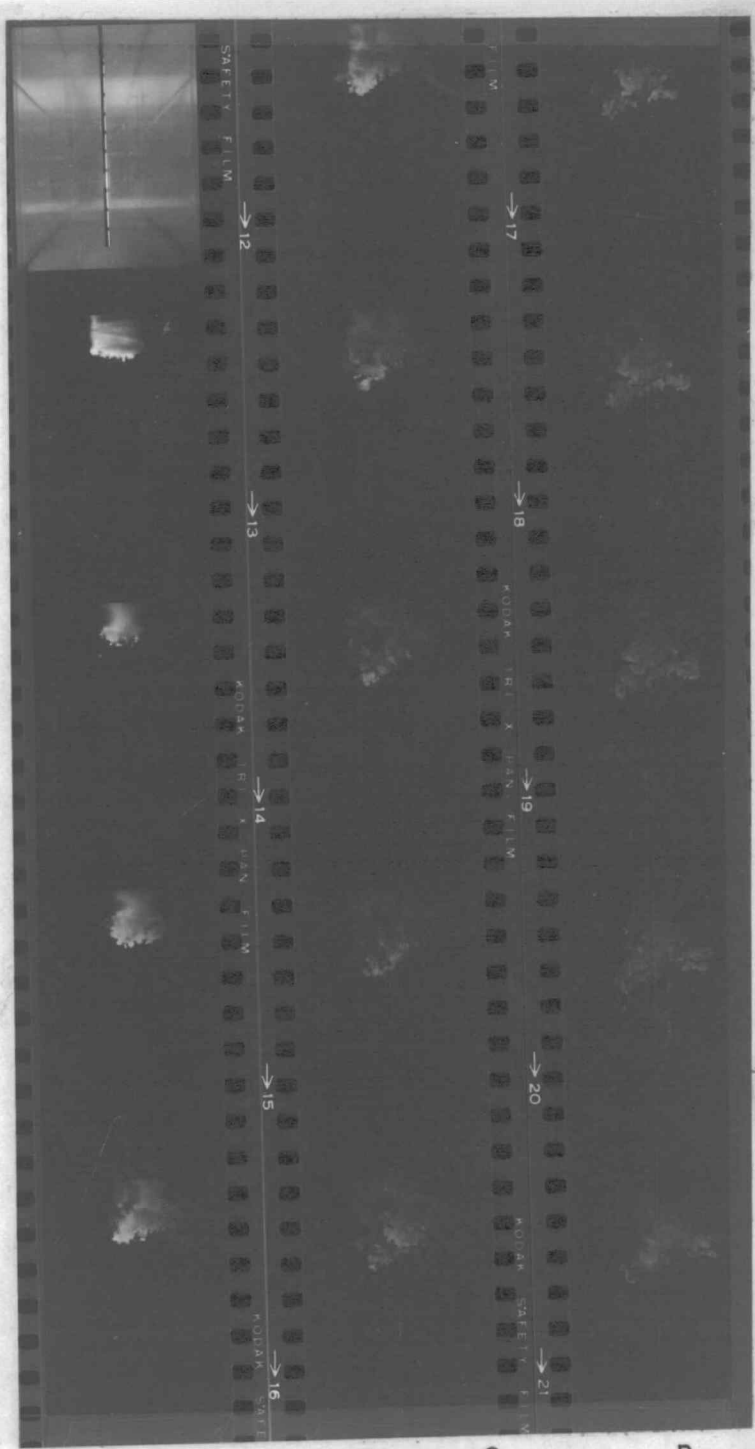

$F = 6.0$ $N = 7$ $\theta_1 = 90^0$ $R = 1.0$

$\frac{X}{X_0} = 7$ $\Delta X/D_0 = 25.10$ EXPOSURE LENGTH = 7.3

PLATE 5 : Cross-sections through buoyant jet for Run 112

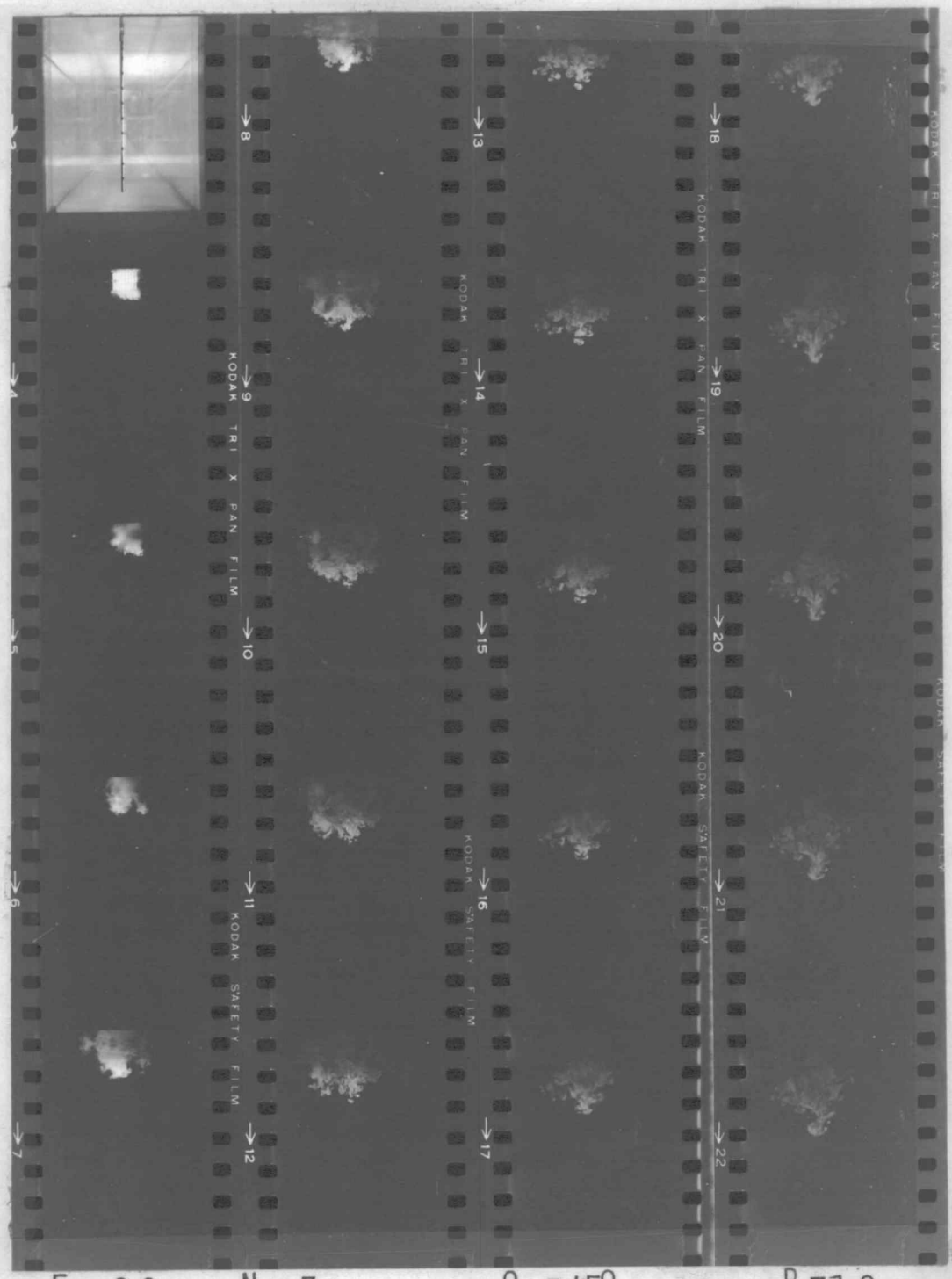

$F = 6.0$ $N = 7$ $\theta_1 = 45^{\circ}$ $R = 1.0$

$\frac{x}{D_0} = 1.0$ $\Delta X/D_0 = 25.3$ EXPOSURE LENGTH = 7.3

PLATE 6 : Cross-sections through buoyant jet for Run 115

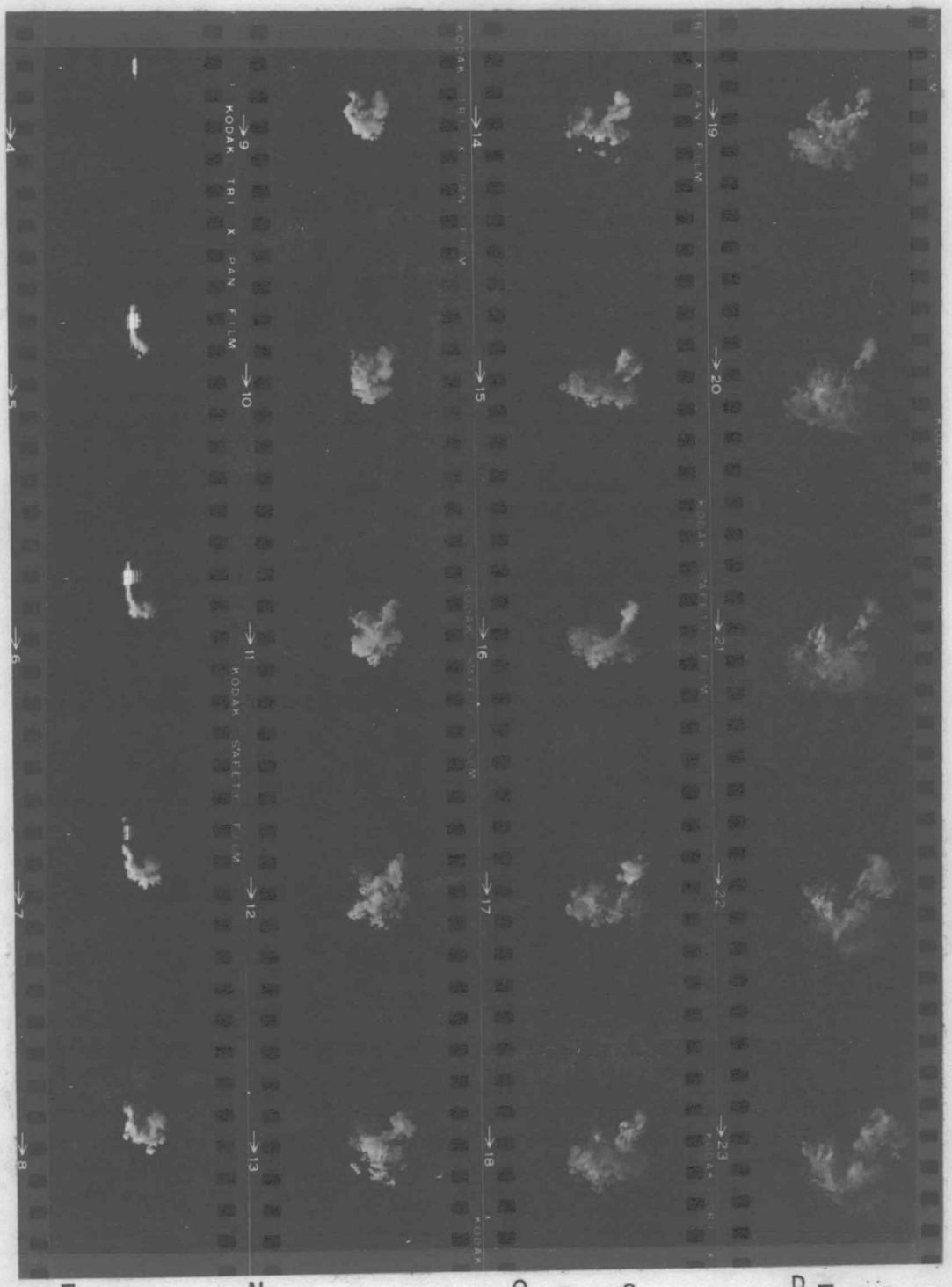

$F = 6.0$ $N = 7$ $\theta_1 = 45^0$ $R = 0.1$

$\frac{y}{\lambda_0} = 0.0$ $\Delta X/D_0 = 2.53$ EXPOSURE LENGTH = 0.73

PLATE 7 : Cross-sections through buoyant jet for Run 116

opposite sides of the channel (Figure 5). The light beams were collimated by slits near each source thus reducing the beam width before reaching the channel slits. In this way only the parallel rays of light from each source were used. A 1000 W quartz-halogen stage light was used on one side, and a 400 W mercury light on the other. Only a 3 mm thick vertical plane in the water perpendicular to the channel walls and direction of towing was illuminated.

Salt water jets discharged from the tank were colored with fluorescein yellow-green color by injecting small amounts of one percent fluorescein dye solution into arbitrary discharge port (Plate 1). or by mixing the dye with salt water in the tank to achieve even concentration in all jets. While the tank was towed, the buoyant jets formed a light yellow-green visible plume. When the laboratory lights were turned off, only the test cross-section was illuminated. Clean tap water was used to fill the channel, so the illuminated section was almost invisible in the absence of dye. When the ports hit the cross-section, the light reflected from them and made them visible. The fluorescein dye in the plume began to glow, but only inside the collimated light beam. As the tank was towed with constant velocity on the rails, the image on this "screen" represented the cross-sections of the buoyant jets in a cross-flow for particular downstream locations, x/D_o. First pictures taken from above the channel with a Polaroid camera using Polaroid black and white film with ASA 3000 speed, were encouraging, so a 35 mm camera was placed at the end of the channel, 4 m in front of the

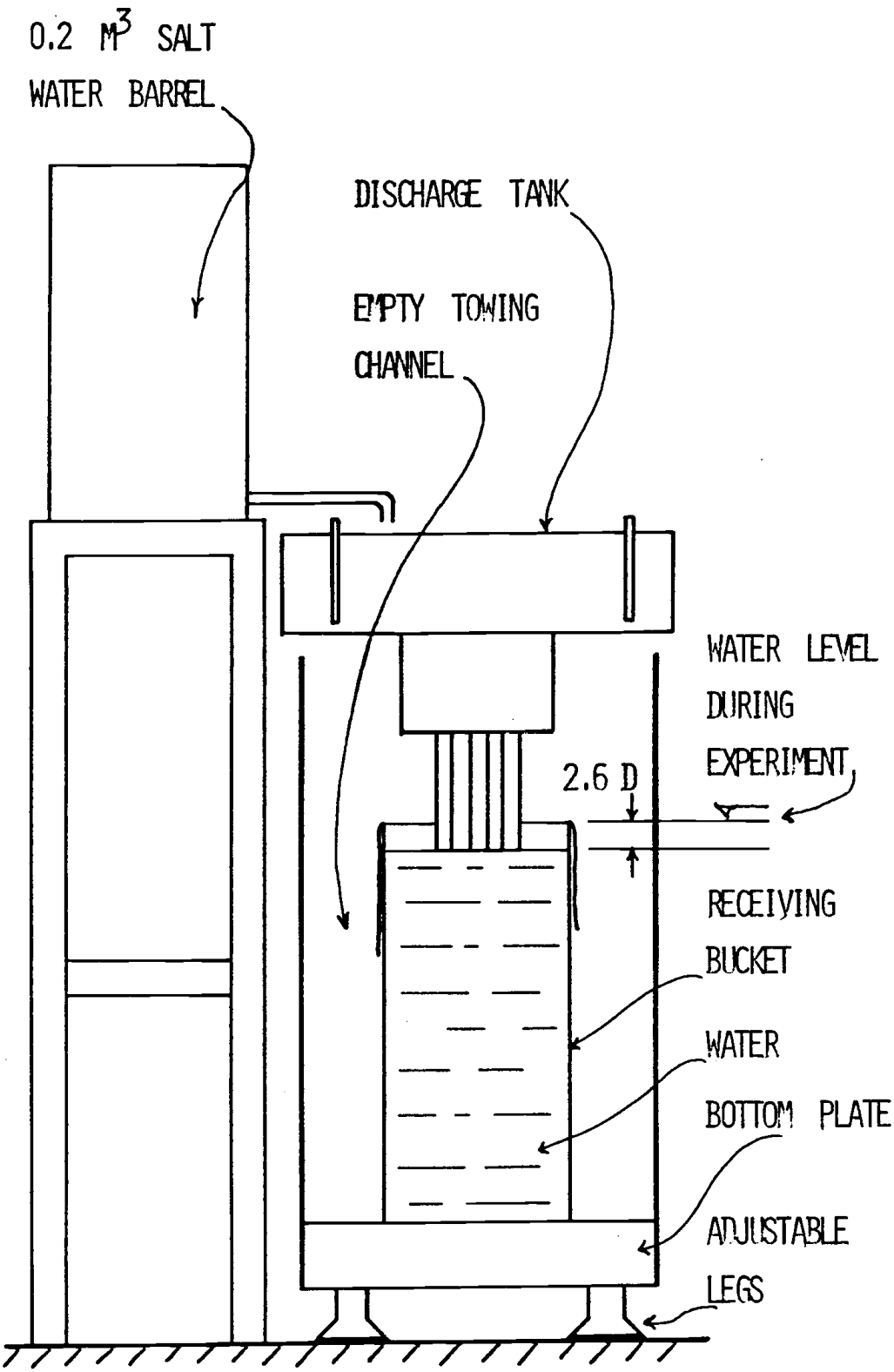

FIGURE 4; Salt water reseryoir and discharge rate calibration setup.

light beam. Pictures were taken using Kodak 2475 Recording Film, processed for approximately ASA 4000 speed, (later on, Kodak 3-x was used with special processing) yet illumination was sufficient only to get pictures of the stagnant jet, since the water absorbed too much light.

The obvious choice was to put the camera closer to the test cross-section. This could be done by submerging the camera in an underwater housing in the channel, but then accurate focusing could not be checked in the viewfinder of the camera, and replacing a roll of new film would be quite tedious. So the author did not hesitate to leave the camera (his own) in the dry "safe" place outside the channel on a tripod and instead, a plane mirror 0.4 m wide and 0.5 m high was inserted 0.9 m in front of the test cross-section. The mirror was placed vertically, oriented at 45 degrees to the symmetry line of the channel, so the light coming from the image was reflected by 90 degrees out through the unmasked portion of the channel to the camera. Because of its size, the mirror was an obstacle in the channel, and the jets were very much disturbed when passing over it, but since the water in the channel, which represented the cross-flow was still, the disturbances from the mirror were not observed in the test cross-section. The bulk of data was collected for downstream distances, x/D_o less than 100. Within this region the flow was not disturbed. Rather, limitations were imposed by the discharge rate, velocity ratio R and size of the channel.

A single lens reflex, 35 mm camera with standard lens 50 mm f 1.4 and attached motor winder was used to record the sequence of images

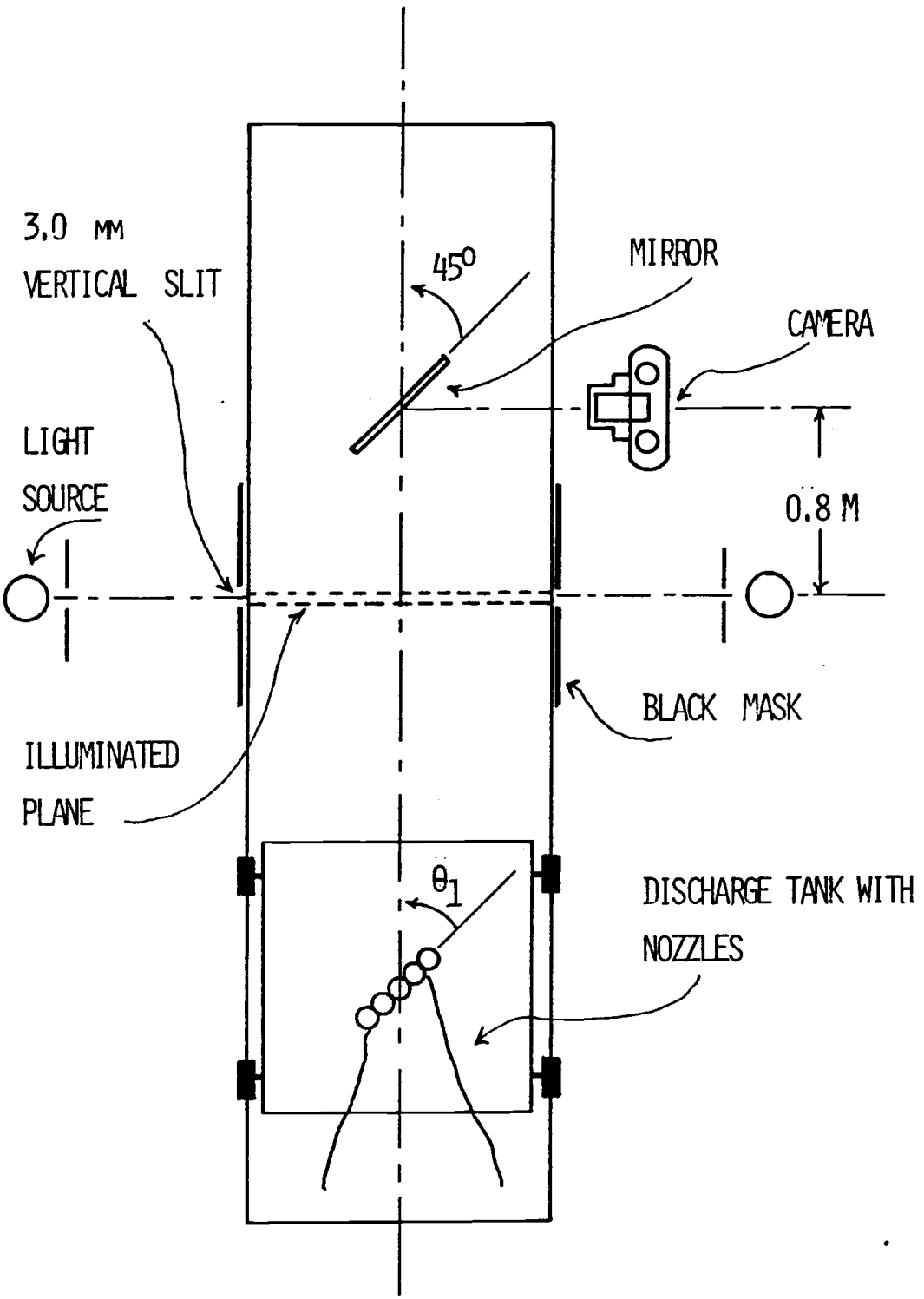

FIGURE 5: Visualization and recording technique.

in the text cross-section. These images were as bright as a picture on a TV screen. The camera was triggered remotely. Once triggered, the interval between the frames was constant with values from 0.6 to 0.9 seconds, depending on the exposure time used.

3.3 Experimental Procedures

It took a few months of enthusiastic trial and error experimentation with available equipment at EPA Corvallis and OSU to get satisfactory results. Once the system was perfected, it took about three hours to make one run (provided the ports were calibrated previously), and twice that time to process the film and reduce the data in numerical form. Most of the runs were made during the weekends or nights, because complete darkness was needed in the lab.

The sequence of steps, called a run, which formed the basic experimental test is enumerated as follows:

1. If there is plenty of salt water skip to step 2. Prepare the salt water in the plastic barrel. (One barrel was sufficient for three to five runs.)
2. If the discharge structure remains the same, skip to step 3. Select desired discharge configuration (N = 7, 5, 3, 2 or 1) and attach it to the plenum chamber on constant velocity head tank in desired orientation with respect to towing (γ = 90, 45, or 0^{o}, irrelevant for single jet).
3. If the control valve is adjusted to give nominal discharge velocity, skip to step 4. Calibrate the control valve in the plenum chamber to yield nominal discharge velocity of U_o = 0.28 m/s.

(Figure 4 shows the arrangement used for valve adjustment. The receiving bucket was placed in the empty channel, below the ports with its upper edge leveled with normal waterlevel, so that the same velocity head was obtained. Control valve was placed in the position which would be known from experience. Discharge flow rate was calculated from the measured time it took a known amount of water to flow from the discharge tank. The amount of water was in turn calculated from the change in water level, and known cross-sectional area of the tank. Discharge velocity was compared to the nominal. When it was close to nominal the calibration/adjustment was completed. Normally this required three to six iterations.)

4. Fill the channel with fresh tap water to the marked level. (This was 2.6 D below port exit.) Volume of water was approximately 5 m^3. Temperature of city water frequently varied for a few degrees C during fill-up, and temperature stratification was observed in the channel while monitoring temperature with a Hewlett-Packard quartz thermometer. To avoid stratification, a pump was used during fill-up to circulate the water in the channel. Water moved along the channel as in a slow flume.

5. If discharge tank is more than two-thirds full skip to step 6. Refill the tank with salt water from the barrel.

6. If temperature difference between water in the tank and water in the channel is less than $0.1^{o}C$, skip to step 7. Adjust the temperature of the salt water in the tank to that of tap

water in the channel to the nearest $0.1^{o}C$. Add cold or warm salt water of the same salt content to the tank and mix. Record the temperatures.

7. Turn off the circulation pump.

8. Calculate the towing velocity from timing the towing of the tank over a known distance. Adjust the speed of the motor drive if velocity is not within desired range. Record the towing velocity.

9. Turn on the mercury lamp (needs time to warm-up).

10. Load the film in the camera, place the camera on the tripod and attach remote release cable. Hang the 1 D diameter and 50 D long reference rod into the center of the test cross-section, focus and take picture of this reference length. Take the rod out. Turn on the motor drive on the camera.

11. Record the water level in the tank.

12. Turn on the 1000 W stage light.

13. Turn off the lights in the laboratory.

14. Unplug the ports and start timing change in water level.

15. Initiate tow.

16. Trigger the camera when the ports hit the illuminated plane and take a sequence of 20 to 28 frames.

17. Turn the lights on, plug the ports and stop timing. Record the time and change in water level in the discharging tank.

18. Turn off both light sources.

19. Open discharge valve to drain the channel.

20. Dismount camera from the tripod and take a picture of all pertinent data for that run.

21. Take a sequence of pictures of stop watch using motor driver to determine interval for this run.

22. Develop film.

Sequences recorded on the film are shown on Plates 4 thru 21. In the darkroom, pictures from the negatives were projected on graph paper with millimeter coordinates. A reference rod was 50D long. A picture of this rod was enlarged to show 25 cm on the paper, such that the scale on the paper was 1D = 5 mm. This scale was then used for data reduction from all frames and all films. Next, the water surface when visible and/or lower edge of ports was used to center the picture on the paper and the contour of film perforation was drawn on the paper. Contours of the image from each frame were traced on the paper, each contour with different color. All subsequent frames were centered according to the marked perforations. Drawings of the contours were superimposed on the first one. Typically two sheets of paper were used for each run, projecting odd numbered frames on one and even numbered on the other to get better clarity. From the frames showing the stop watch, the average time between two frames was calculated for each run. Distance between two frames was calculated from known towing velocity, and a downstream distance X/D_0 was assigned to each frame.

The initial X/D_0 was established from analyses of the first four frames and known towing velocity.

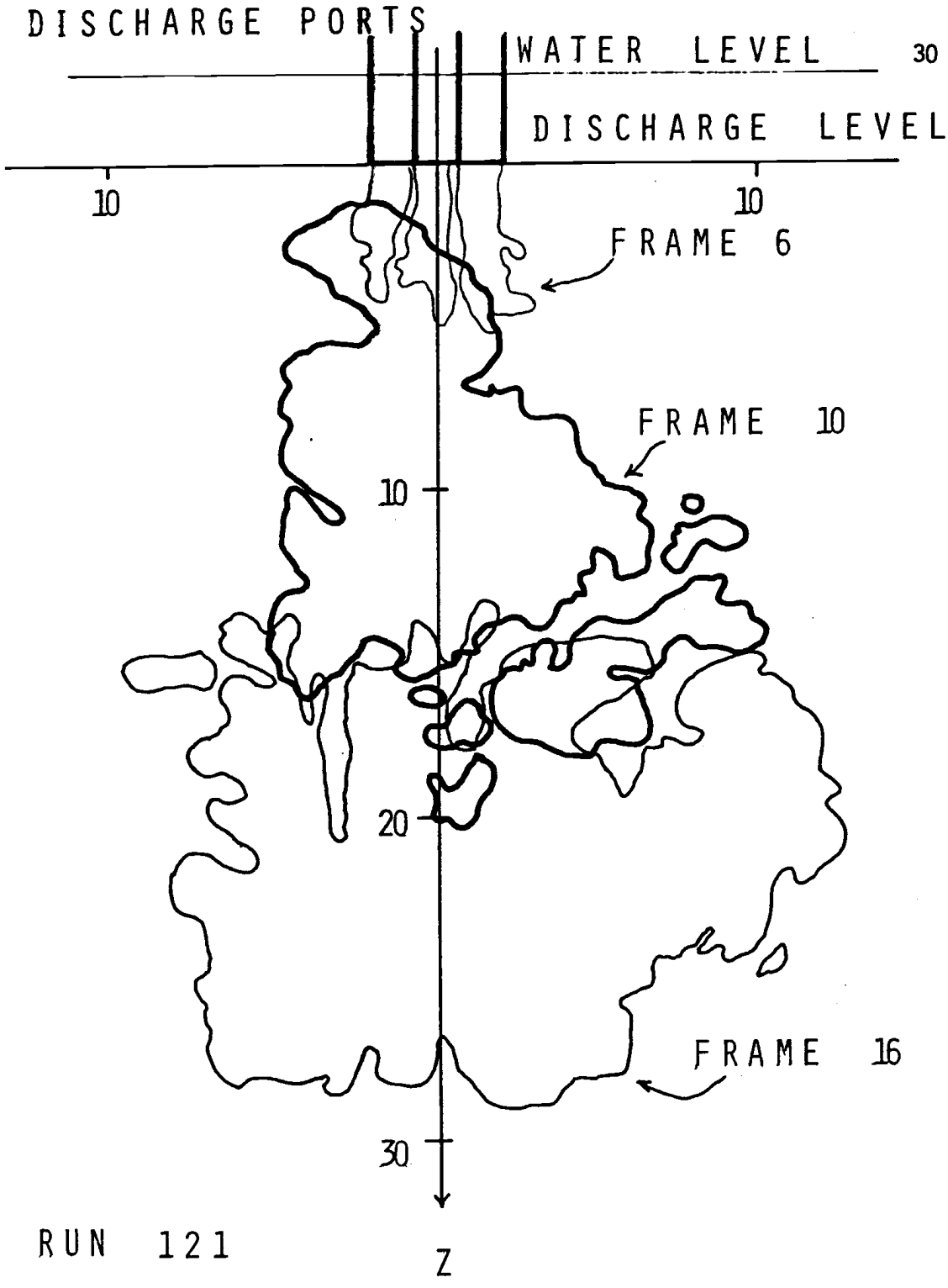

FIGURE 6: Contours of the Cross-section on the graph paper.

The upper edge, Z_{max}, lower edge, Z_{min}, horizontal width, W/D_o, and areas were measured for each frame and tabulated (Table 1). Figure 6 shows the method of data reduction from millimeter paper. (Only frames 6, 10,and 16 are shown for clarity.)

The centerline of the trajectories was assumed to be in the middle between upper and lower edges of the plume, and it was calculated from tabulated Z_{max} and Z_{min}. Vertical width B was obtained from the difference between Z_{max} and Z_{min}. Cross-sectional areas A_x at a particular downstream location x/D_o were non-dimensionalized with respect to the initial discharge cross-section for particular number of ports. Densimetric Froude number was calculated from measured water temperatures (T_o, T_a), jet velocity U_o and known salinity s.

IV. RESULTS

4.1 General

The main objective of this investigation was to find characteristics of merging buoyant jets in crossflow.

Independent variables and their nominal values considered in the experiments were:

Variable	Symbol	Nominal values
Number of ports	N	7, 5, 3, 2, 1
Velocity ratio	R	0.1, 0.2, 0.5, 1.0
Angle between crossflow and line connecting the ports	θ_1	90, 45, 0°

This could yield broad spectrum of data. Not all cases were covered by the experiments. Seventeen experiments were analyzed in detail. They can be grouped into three families, with one parameter varying and two fixed.

N = 7 θ_1=90	R = 0.1	0.2	0.5	1.0	
	Run 131, 117$_a$	129, 111	130, 111	112	
	N = 1	2	3	5	7
R = 0.2 θ_1=90	Run 125, 128	123, 129	121, 122	119, 120	129, 111
	θ =	0	45	90	
R = 0.2, N=7	Run	133	132	129, 111	

Totally 32 runs were made with crossflow.

Table 1 summarizes all measured and calculated variables for each run.

Run	N	θ_1	U_o	U_∞	R	T_a	T_o	g'	F	$\frac{x_o}{D_o}$	$\frac{\Delta_x}{D_o}$	$\frac{ex1}{D_o}$	Re
106a	7	0	27.9	14.00	0.501	15.20	15.20	0.2260	6.01	0.0	9.30	3.50	2658
106b	7	0	27.9	14.00	0.501	14.92	14.65	0.2268	6.00	0.0	9.30	3.50	2658
107	7	0	27.9	14.00	0.501	14.10	13.71	0.2274	5.99	0.0	9.30	3.50	2658
108	7	0	27.9	14.00	0.501	15.30	15.50	0.2256	6.02	0.0	12.35	3.50	2658
109	7	0	27.9	27.90	1.000	16.14	16.28	0.2255	6.02	0.0	24.7	6.98	2658
110	7	90	27.9	5.60	0.201	15.43	15.34	0.2262	6.01	0.0	5.03	1.47	2658
111	7	90	27.9	13.75	0.493	16.74	16.71	0.2254	6.02	4	12.05	3.61	2658
112	7	90	27.9	28.98	1.039	14.05	14.09	0.2267	6.00	7	25.1	7.3	2658
113	7	45	27.9	5.60	0.201	13.79	13.24	0.3380	5.99		4.08	1.47	2658
114	7	45	27.9	13.89	0.498	14.28	14.38	0.2241	6.04		12.4	3.50	2658
115	7	45	27.9	27.90	1.000	15.13	15.00	0.2264	6.01		25.25	6.98	2658
116	7	45	27.9	27.90	0.100	15.32	15.17	0.2264	6.01		2.53	6.98	2658
117a	7	90	27.9	2.80	0.100	14.22	14.23	0.2266	6.00	0	2.56	0.73	2658
117b	7	90	27.9	2.80	0.100	14.11	14.01	0.2269	6.00		2.57	0.70	2658

Table 1: Summary of most important data for each run.

Run	N	θ_1	U_o	U_∞	R	T_a	T_o	g'	F	$\frac{w_o}{D_o}$	$\frac{\Delta_x}{D_o}$	$\frac{ex1}{D_o}$	Re
118	5	90	27.85	2.8	0.100	14.01	14.20	0.2264	6.00	0.0	2.58	0.7	2659
119	5	90	27.85	5.7	0.203	14.01	14.08	0.2267	5.99	1.5	5.20	1.48	2659
120	5	90	27.85	5.7	0.203	14.07	14.02	0.2268	5.99	0.5	5.07	1.49	2659
121	3	90	27.30	5.6	0.204	15.33	15.28	0.2262	5.88	0.0	4.98	1.46	2659
122	3	90	27.30	5.6	0.206	15.17	15.20	0.2260	5.88	1.0	5.20	1.47	2610
123	2	90	28.25	5.5	0.195	15.28	15.49	0.2257	6.09	1.0	5.02	1.45	2610
124	2	90	28.25	5.5	0.195	14.53	14.38	0.2247	6.11	1.0	5.18	1.46	2692
125	1	--	28.05	5.57	0.199	15.94	15.93	0.2258	6.05	0.5	5.15	1.46	2692
126	1	--	28.05	13.99	0.499	15.51	15.50	0.2256	6.05	0.0	13.20	3.5	2673
127	1	--	28.05	2.8	0.100	19.10	19.05	0.2254	6.05	0.0	2.65	0.7	2673
128	1	--	29.05	5.71	0.204	18.86	18.86	0.2246	6.06	0.5	5.18	1.50	2768
129	7	90	28.15	5.53	0.197	18.06	18.13	0.2245	6.09	0.0	4.65	1.45	2682
130b	7	90	28.15	14.16	0.505	18.67	18.71	0.2243	6.09	0.0	12.00	3.75	2682
131	7	90	28.15	2.7	0.097	18.60	18.59	0.2246	6.09	0.5	2.33	0.71	2682
132	7	45	28.15	5.5	0.197	18.47	18.41	0.2246	6.09	0.5	4.70	1.45	2682
133	7	0	28.15	5.6	0.199	18.52	18.48	0.2245	6.09	0.0	4.68	1.46	2682
134	7	0	28.15	2.8	0.100	15.62	15.50	0.2261	6.06	0.0	2.63	0.0	2682
135	7	0	28.15	5.6	0.198	15.58	15.54	0.2261	6.06	0.0	5.13	0.0	2682

Table 1: Summary of most important data for each run (continued)

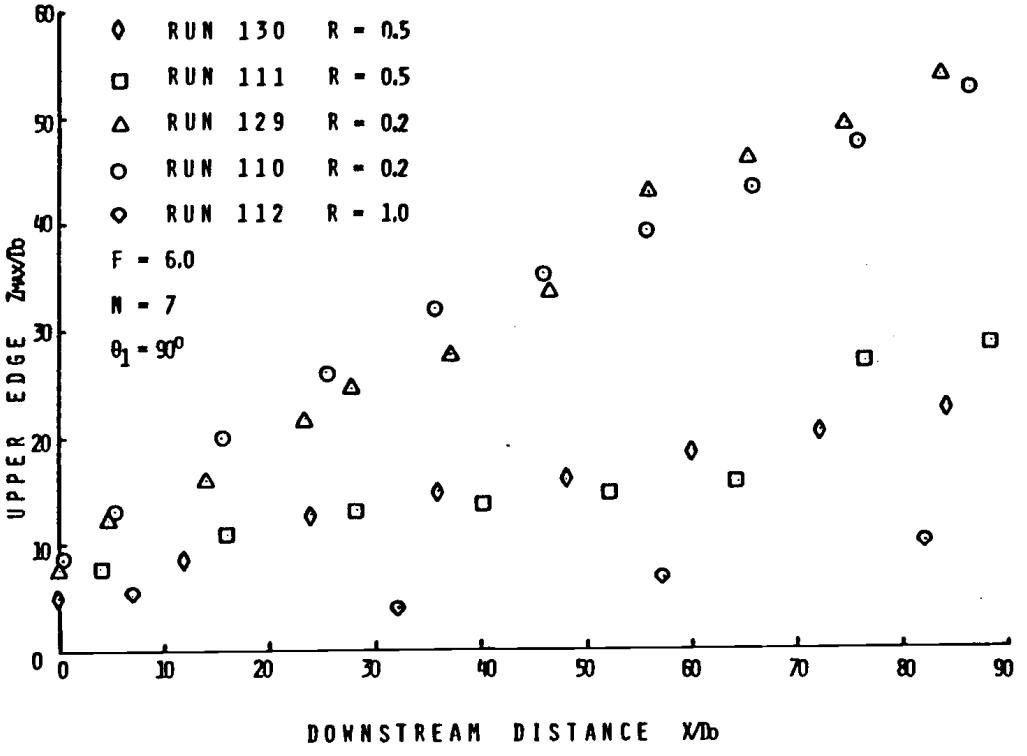

FIGURE 7: Effect of R on Upper Edge Trajectory for F=6.0, N=7, $\theta_1=90^0$

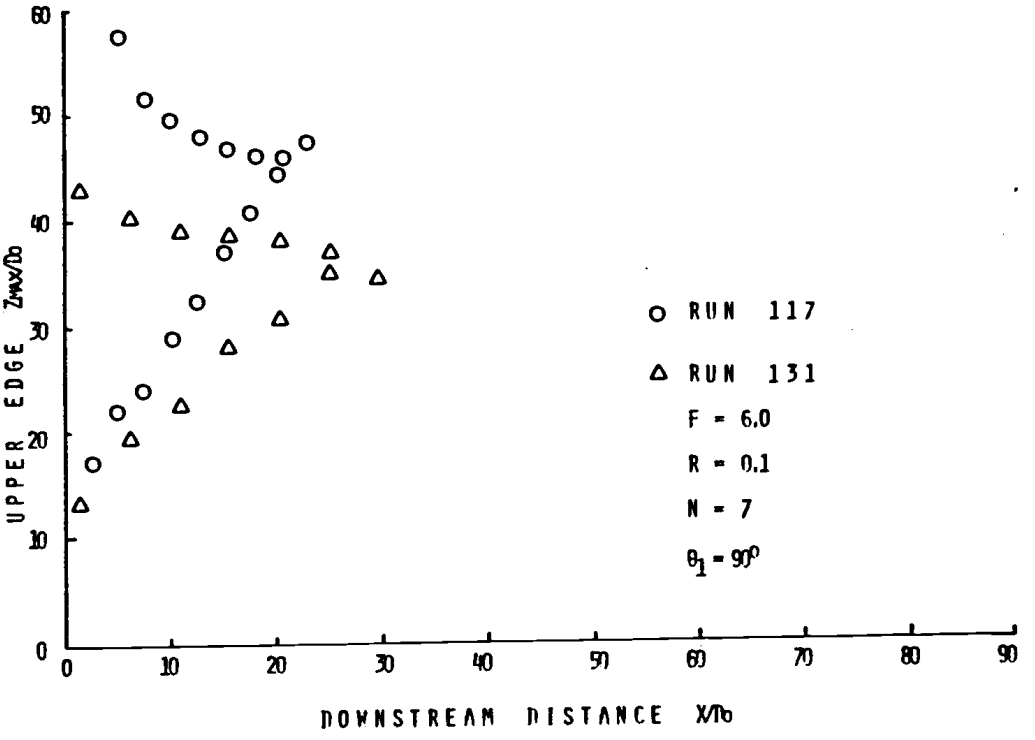

FIGURE 8: Upper Edge Trajectory for F=6.0, N=7, $\theta_1=90^0$, R=0.1

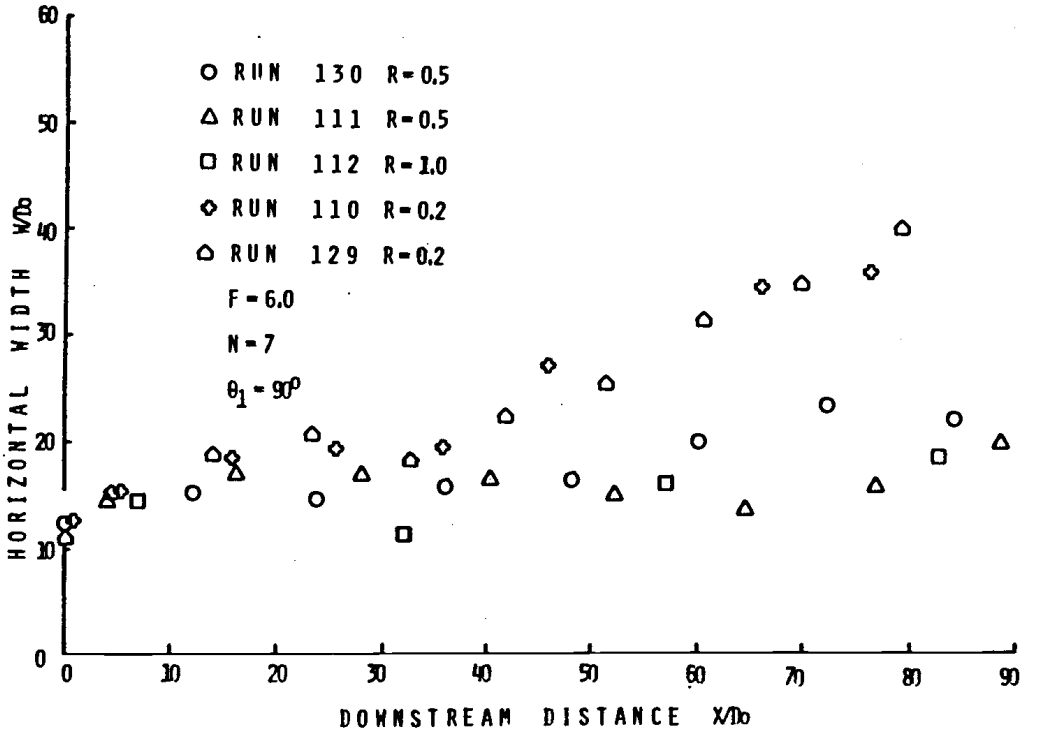

FIGURE 9: Effect of R on Horizontal Width for F=6.0, N=7, $\theta_1=90^0$

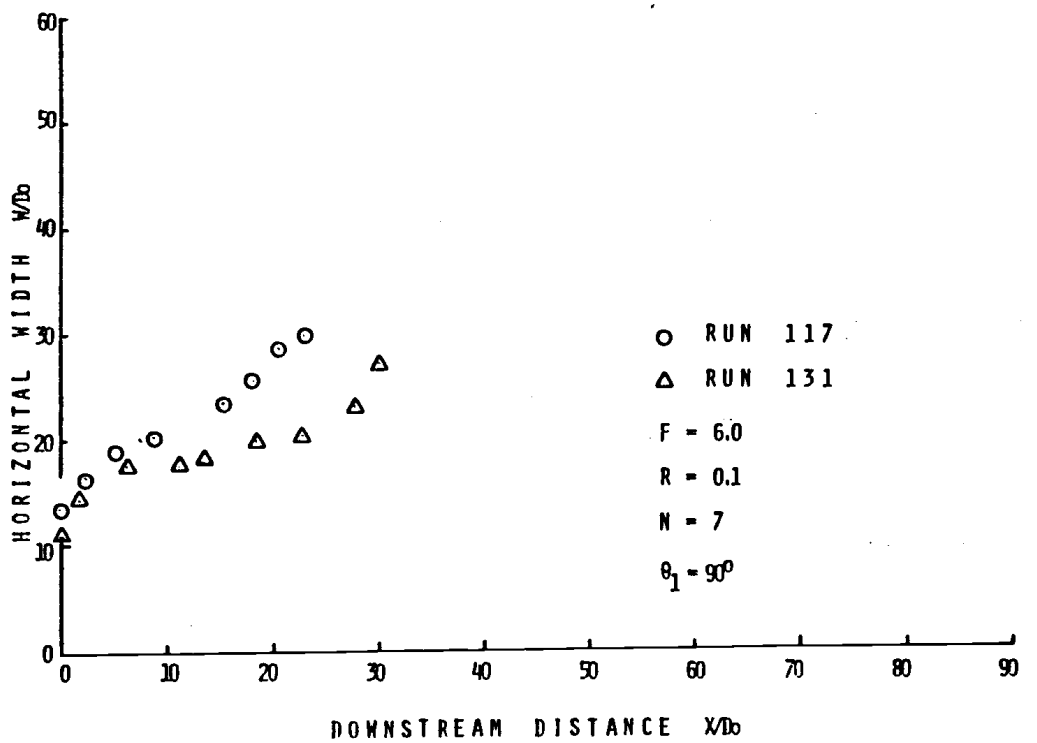

FIGURE 10: Horizontal Width for F=6.0, N=7, $\theta_1=90^0$, R=0.1

Only the edge of the plume furtherest from discharge was analyzed in detail, though data for centerline and lower edge were also reduced and tabulated in Table 2. The upper edge was always sharp and clearly visible, so it was not difficult to trace the contour on the paper. The lower edge was fuzzy in many cases, due to several effects. First, the light from it travelled through nonhomogeneous medium due to dyed jets which were moving towards the mirror. These jets did not block the light path, but distorted the lower part of the illuminated image slightly. By lower is meant the position closer to the ports, and should not be confused by the fact that pictures were taken in the channel with the vertical axis pointing downward. The upper edge was always sharp since the water was clean and undisturbed in that light path. Secondly, the jets acted somewhat like a solid body in the flow, producing wake and vortex shedding effects behind. Sometimes it was difficult to distinguish the contour of main plume cross-section and wake (Plate 5). Extreme readings were reduced from the pictures. Sheding phenomenon is captured on the photograph Plate 3 which was taken from above the channel. In this case only plane 10 D below the ports, parallel to water surface was illuminated. The dimension on the pictures are distorted since the camera was mounted at 45° towards the water surface. Yet, the wake effect of the jets is clearly seen and one can even observe the vortex street. Ports were submerged 2.6 D below the water surface. On this basis one can argue now, that

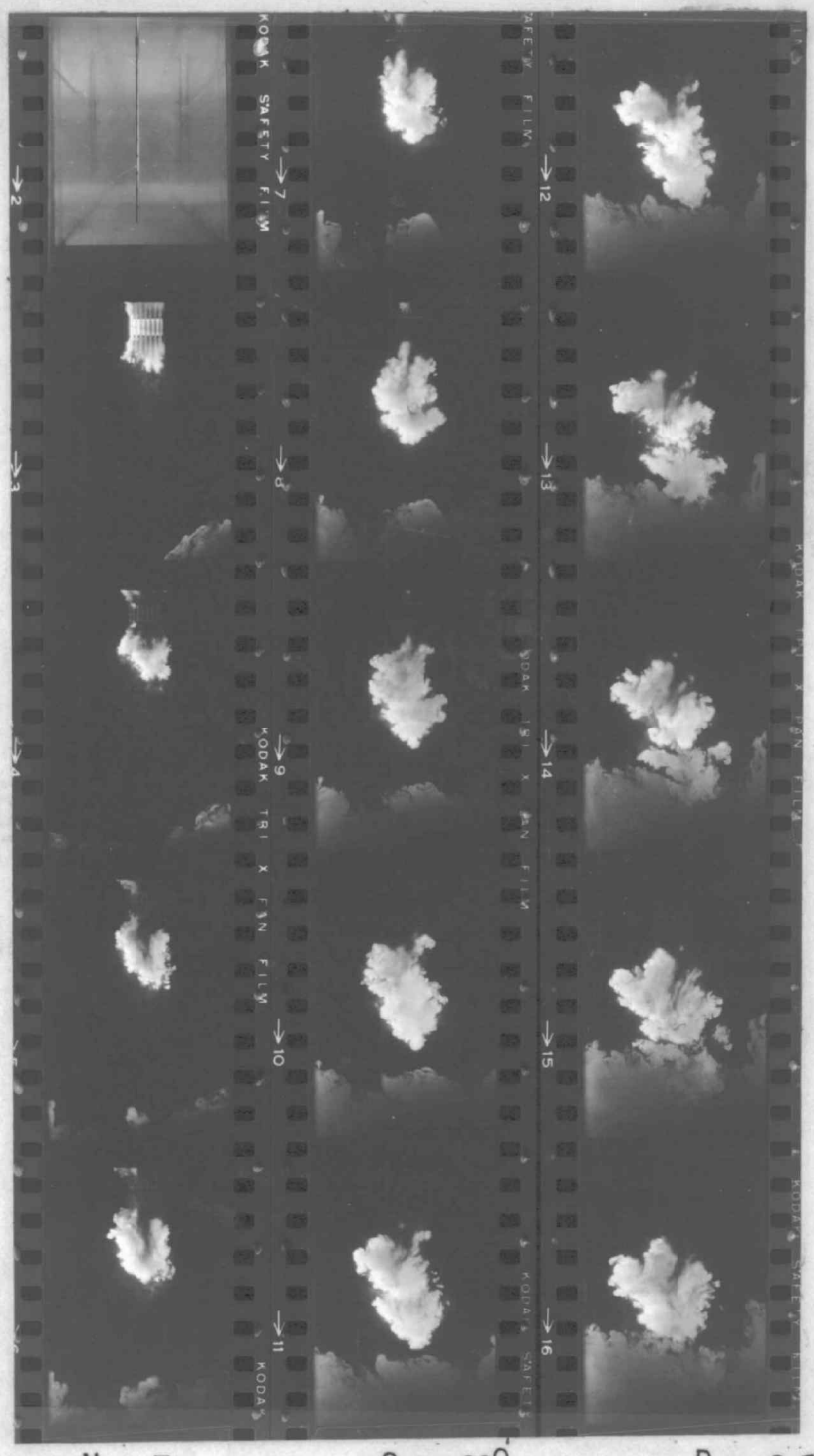

F = 6.0 N = 7 $\theta_1 = 90^0$ R = 0.1

$\frac{x}{\lambda_0} = 0.0$ $\Delta X/D_0 = 2.56$ EXPOSURE LENGTH = 0.73

PLATE 8 ; Cross-sections through buoyant jet for Run 117a

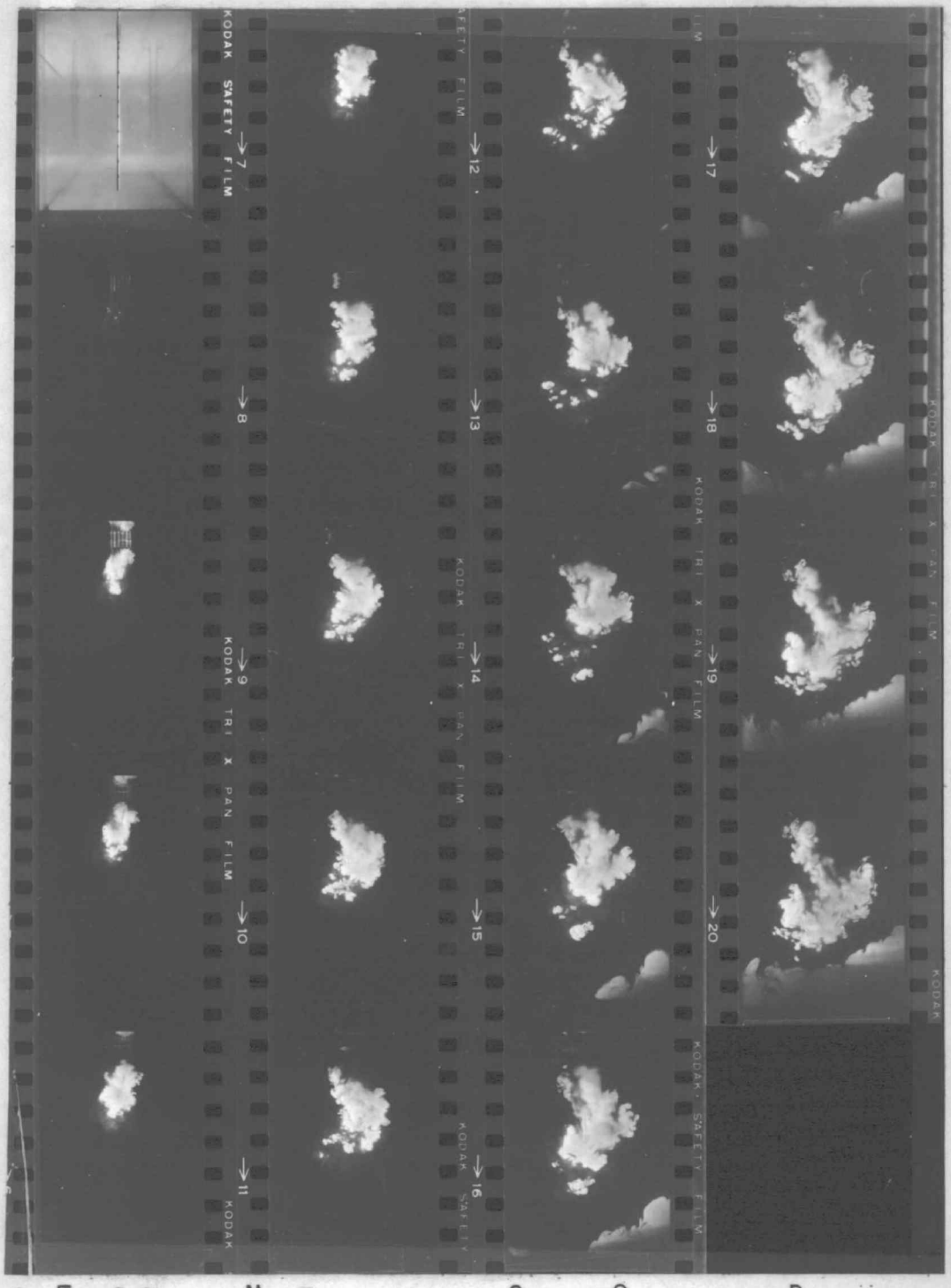

$F = 6.0$ $N = 5$ $\theta_1 = 90^0$ $R = 0.1$

$X_0 = -0.5$ $\Delta X/D_0 = 2.58$ EXPOSURE LENGTH = 0.72

PLATE 9 : Cross-sections through buoyant jet for Run 118

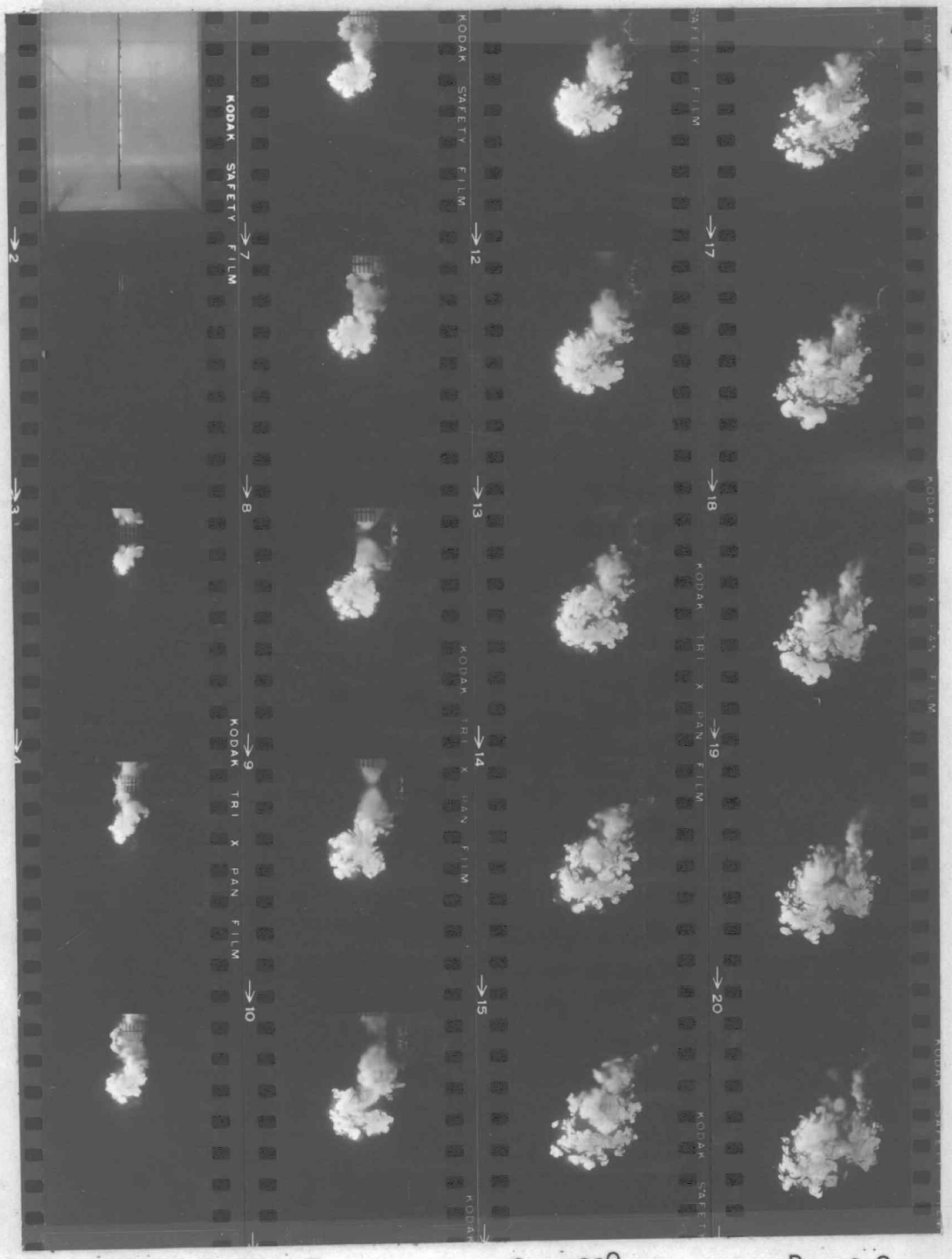

$F = 6.0$ $N = 5$ $\theta_1 = 90^0$ $R = 0.2$

$\frac{Y}{Y_0} = 1.5$ (FRAME 4) $\Delta X/D_0 = 5.2$ EXPOSURE LENGTH = 1.48

PLATE 10 : Cross-sections through buoyant jet for Run 119

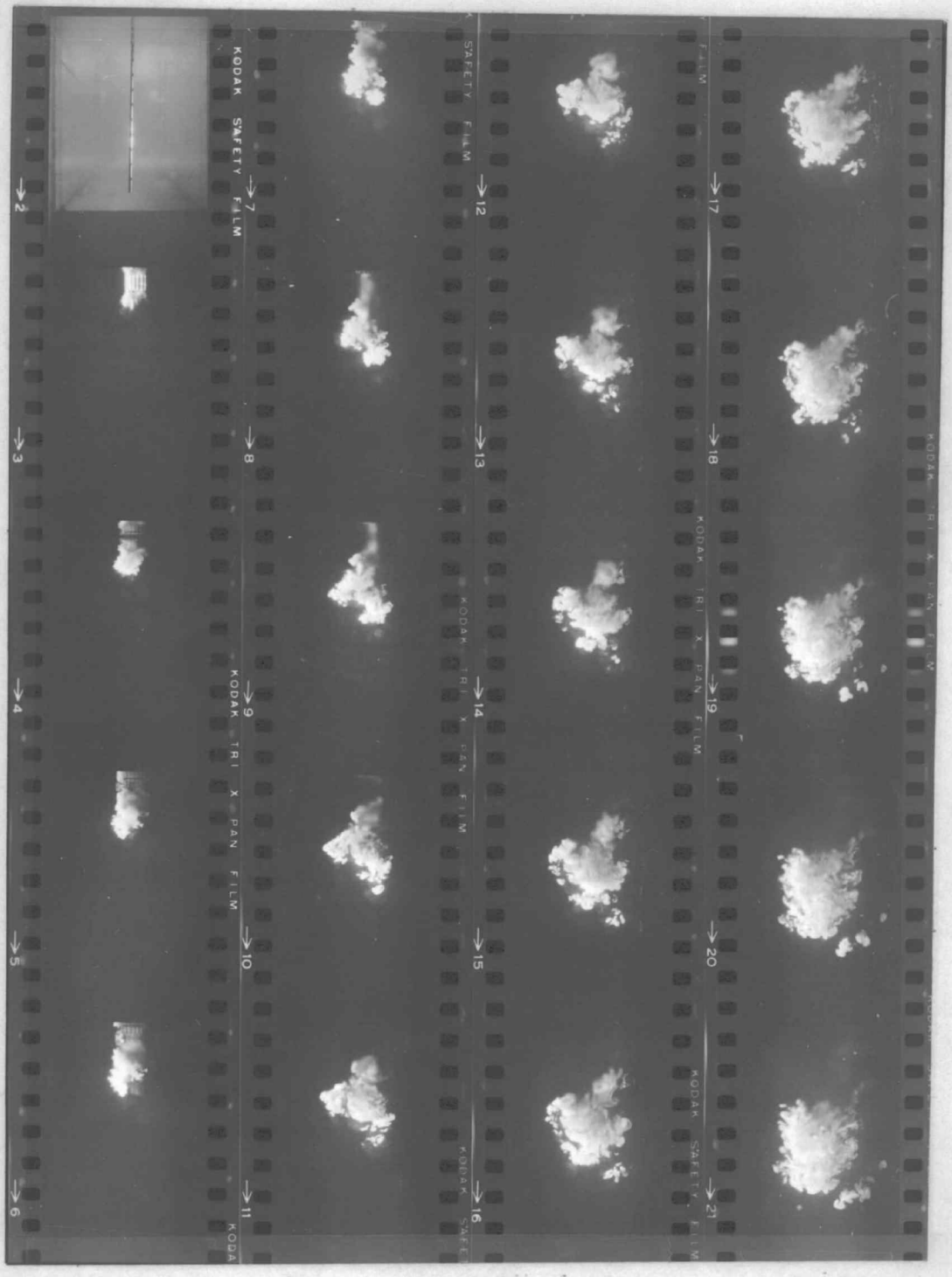

$F = 6.0$ $N = 5$ $\theta_1 = 90^0$ $R = 0.2$

$\frac{Y}{Y_0} = 0.5$ $\Delta X/D_0 = 5.07$ EXPOSURE LENGTH = 1.48

PLATE 11 : Cross-sections through buoyant jet for Run 120

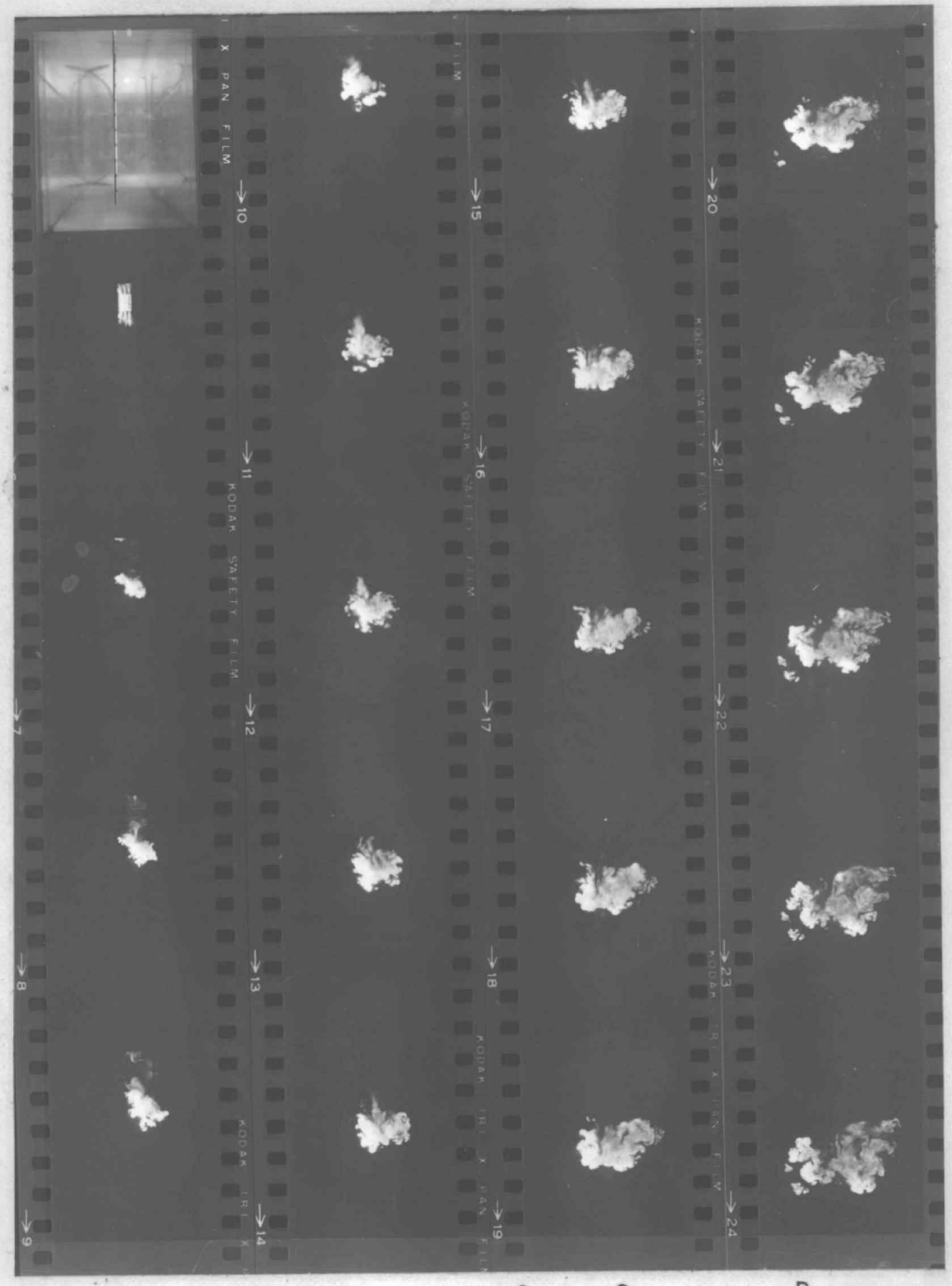

F = 6.0 N = 3 $\theta_1 = 90^0$ R = 0.2

$X/D_0 = 0.0$ $\Delta X/D_0 = 4.98$ EXPOSURE LENGTH = 1.46

PLATE 12 ; Cross-sections through buoyant jet for Run 121

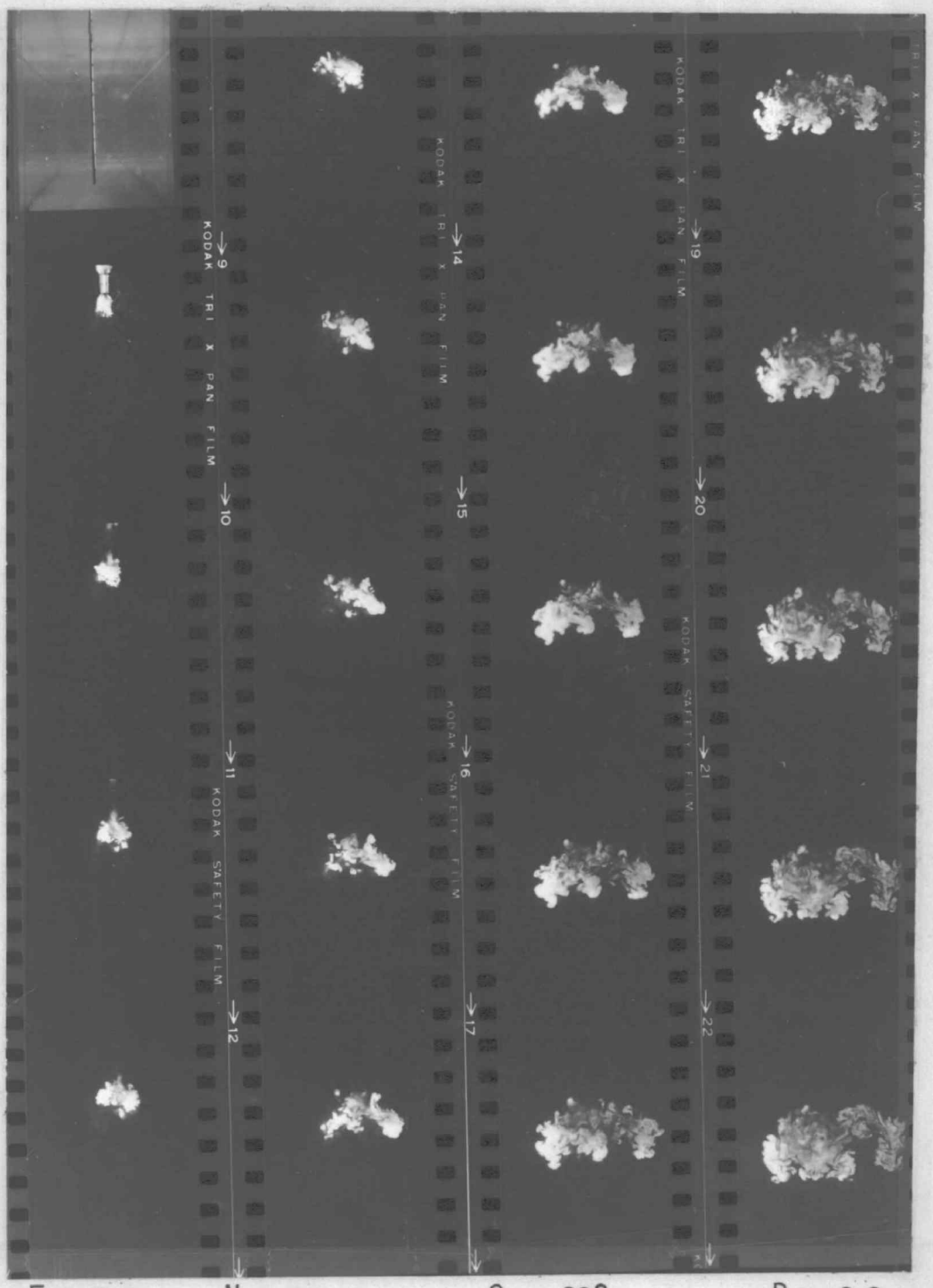

$F = 6.0$ $N = 2$ $\theta_1 = 90°$ $R = 0.2$

$\frac{x}{\lambda_0} = 1.0$ $\Delta X/D_0 = 5.0$ EXPOSURE LENGTH = 1.45

PLATE 13 ; Cross-sections through buoyant jet for Run 123

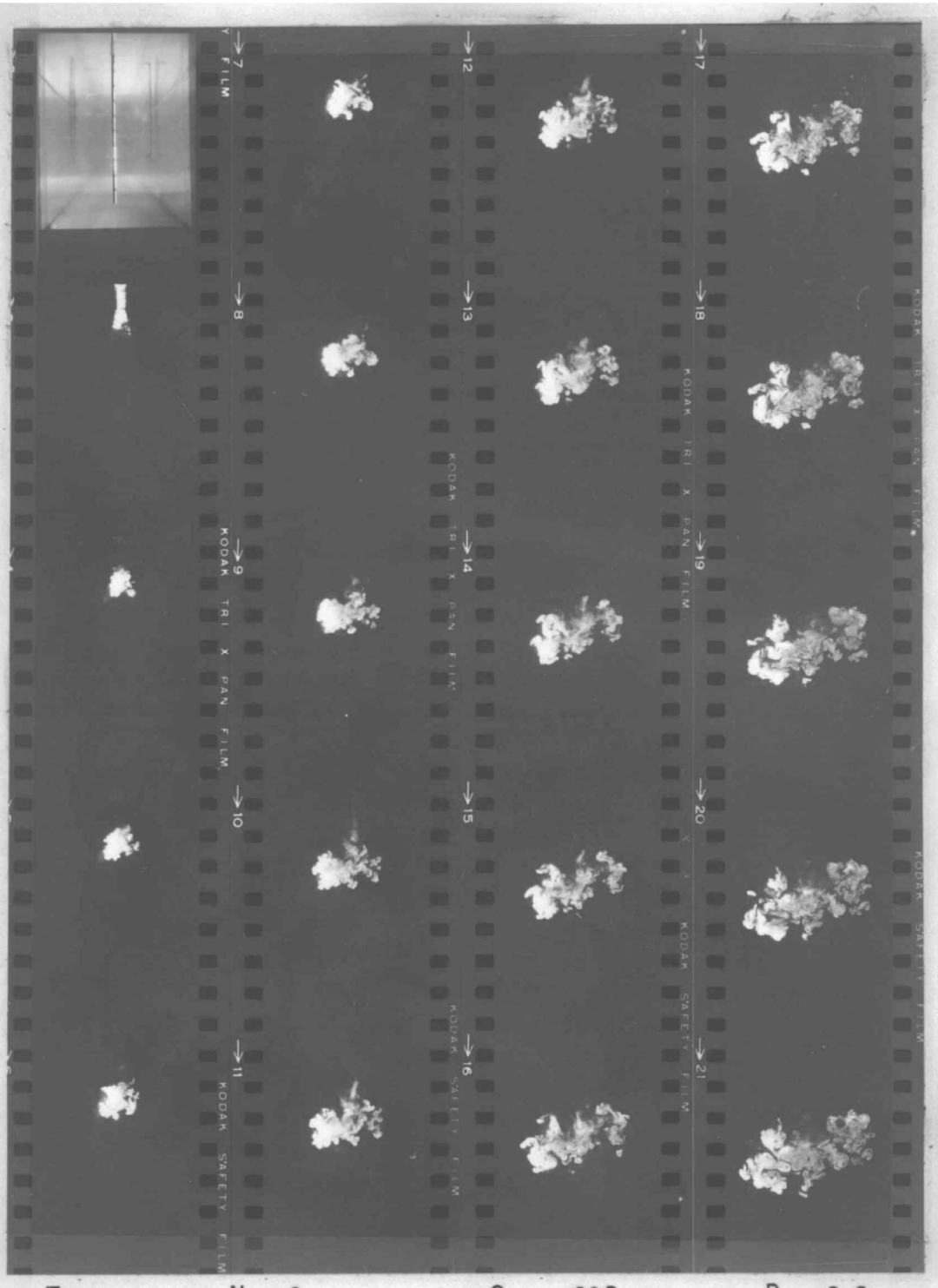

$F = 6.0$ $N = 2$ $\theta_1 = 90°$ $R = 0.2$

$x/D_0 = 1.0$ $\Delta X/D_0 = 5.2$ EXPOSURE LENGTH = 1.46

PLATE 14 : Cross-sections through buoyant jet for Run 124

the shedding is due to the ports themselves. This was checked in an experiment with no jets discharging, and with channel water contanimated with fluorescein dye from previous run. The light plane showed patterns of very slowly moving ambient currents. So, when the ports were travelling with the same speed as before, no disturbance was observed in the pattern 10 D below the ports. A slight wake was caused by the ports, but limited to the area between the port exit and water surface. It was very strong for R = 1.0 when the plumes were downwashed completely. It was also seen 10 to 20 D behind the ports at R = 0.5.

4.2 Effects of Velocity

The upper edge trajectories of buoyant merging jets (Figures 8 and 9) for the same geometry (N = 7, $\theta_1 = 90^o$, L/D = 1.33) can be described as follows. Jets discharge vertically into a crossflow, raise to a certain height, depending on velocity ratio R, next they deflect with the crossflow. From the downstream distance of 10 D the trajectory seem to be a straight line for all velocity ratios.

Tests at R = 0.1 show that the discharge rate was too high for the size of the towing channel. For this case only, recording below 20 D are good. Plates 8 and 9 show the boundary effect.

Horizontal width W/D (Figures 9 and 10) for (N = 7, $\theta_1 = 90^o$, L/D = 1.33) depend on velocity ratio in the same way as the upper edge. The width reduces with increasing velocity. Width data are

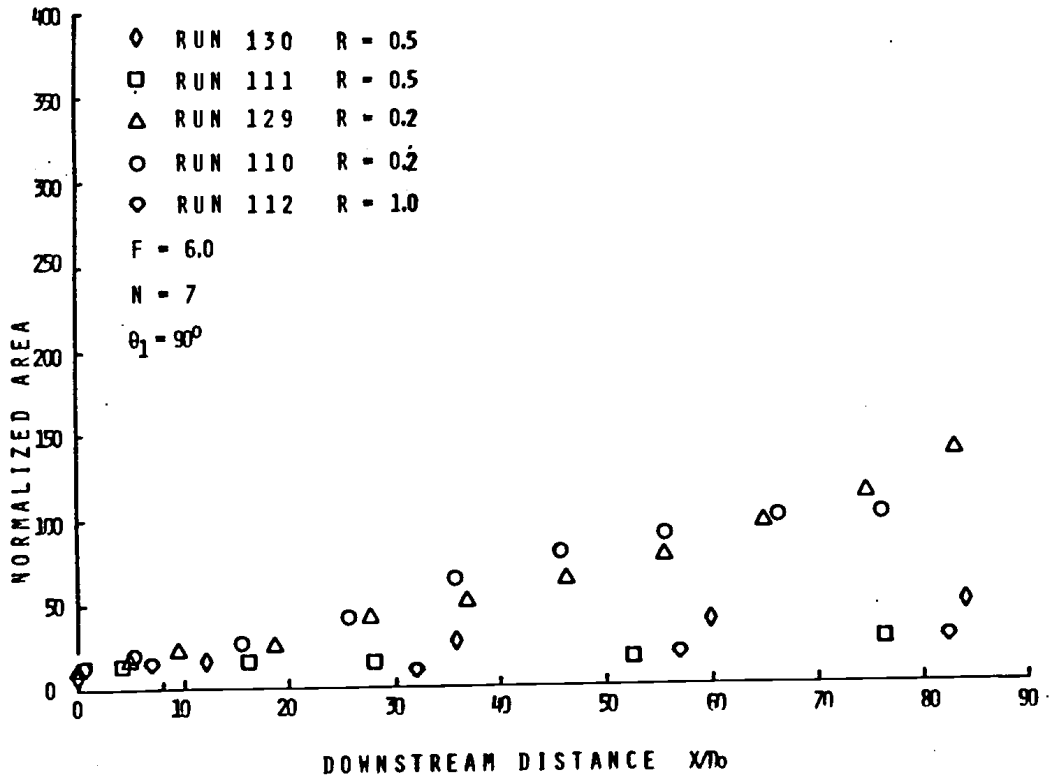

FIGURE 11: Effect of R on Normalized Area for F=6.0, N=7, $\theta_1=90^0$

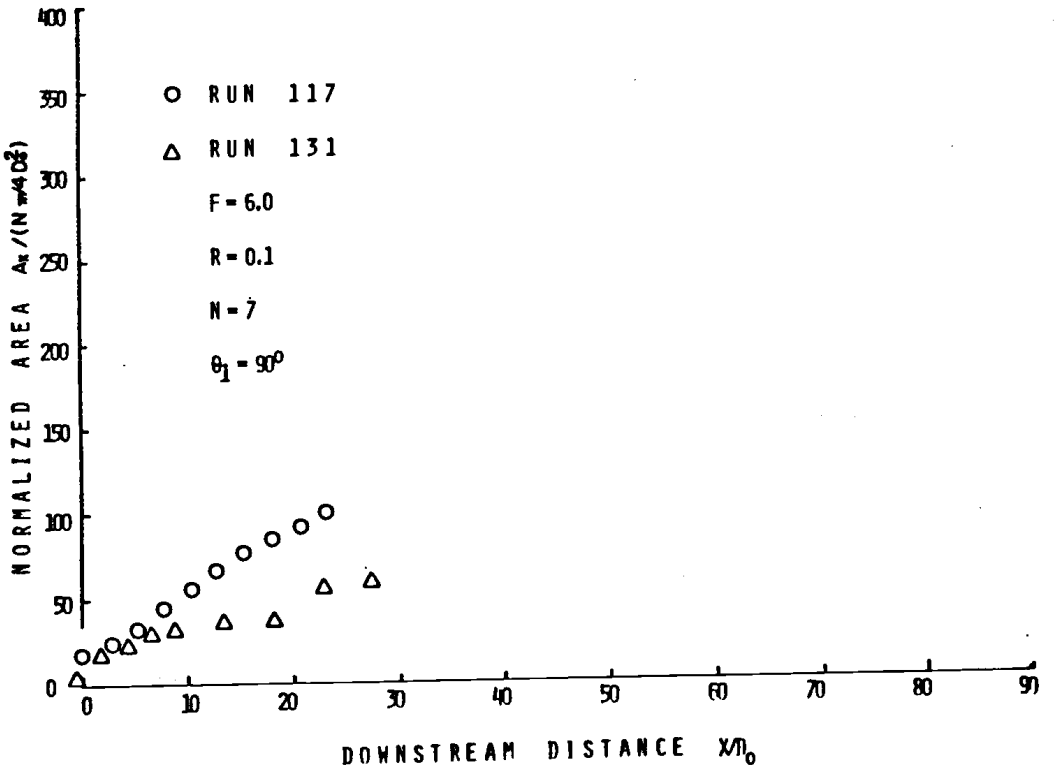

FIGURE 12: Normalized Area for F=6.0, N=7, $\theta_1=90^0$

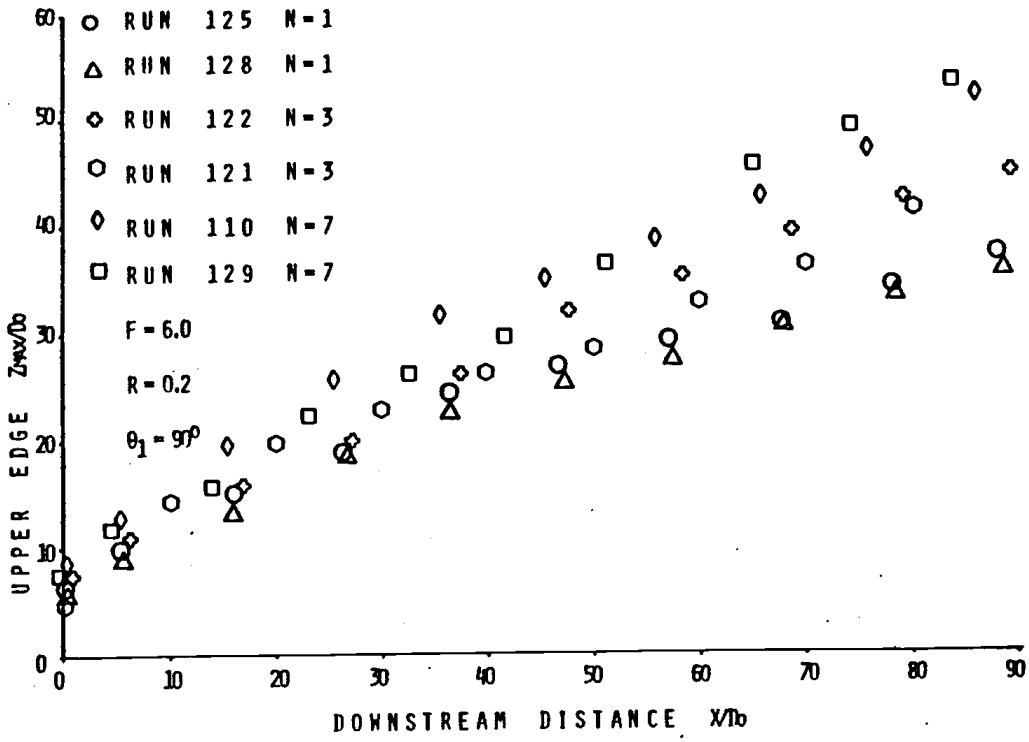

FIGURE 13: Effect of N on Upper Edge Trajectory for F=6.0, θ_1=90°, R=0.2, N=1,3,7

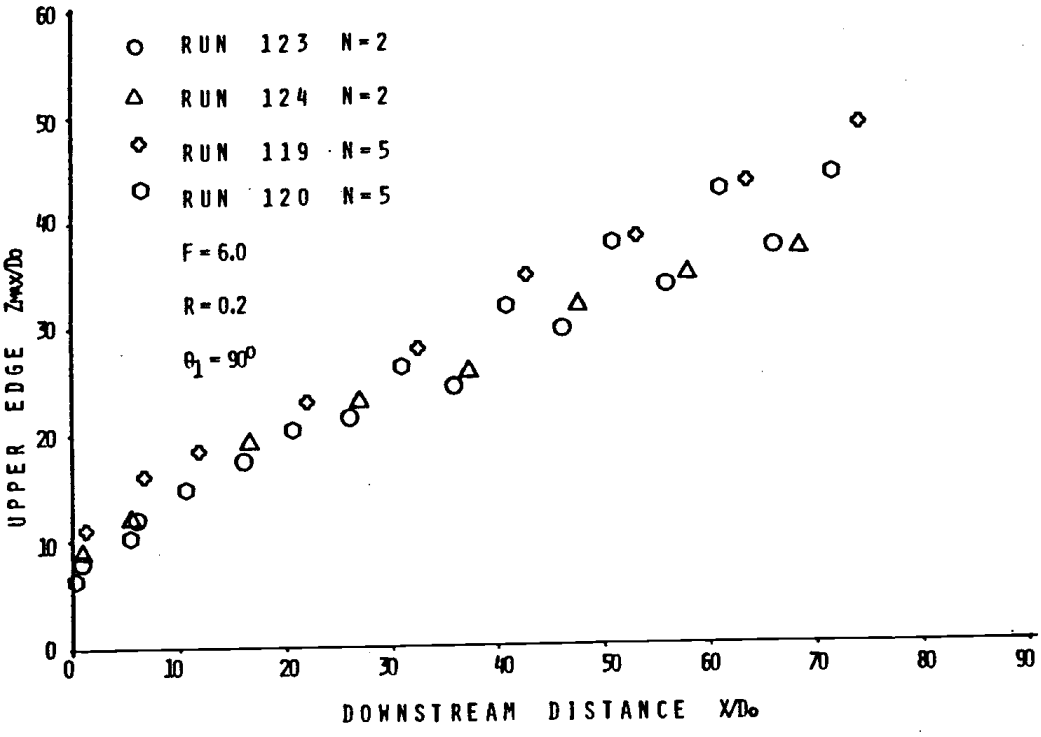

FIGURE 14: Effect of N on Upper Edge Trajectory for F=6.0, θ_1=90°, R=0.2, N=2,5

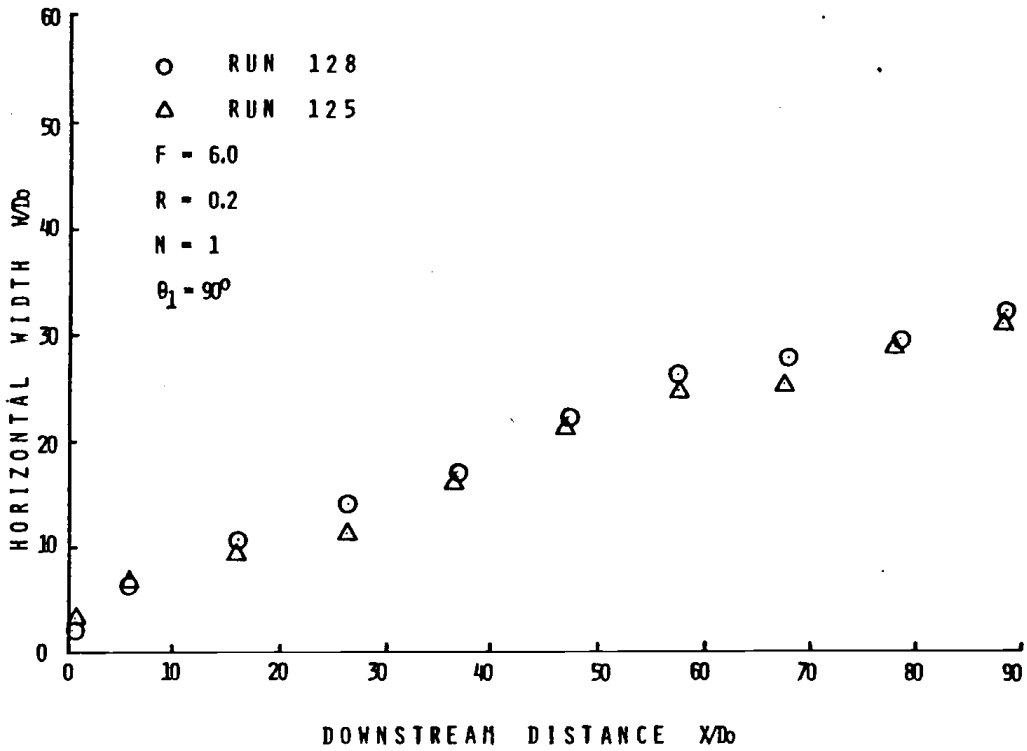

FIGURE 15: Horizontal Width for F=6.0, R=0.2, θ_1=90°, N=1

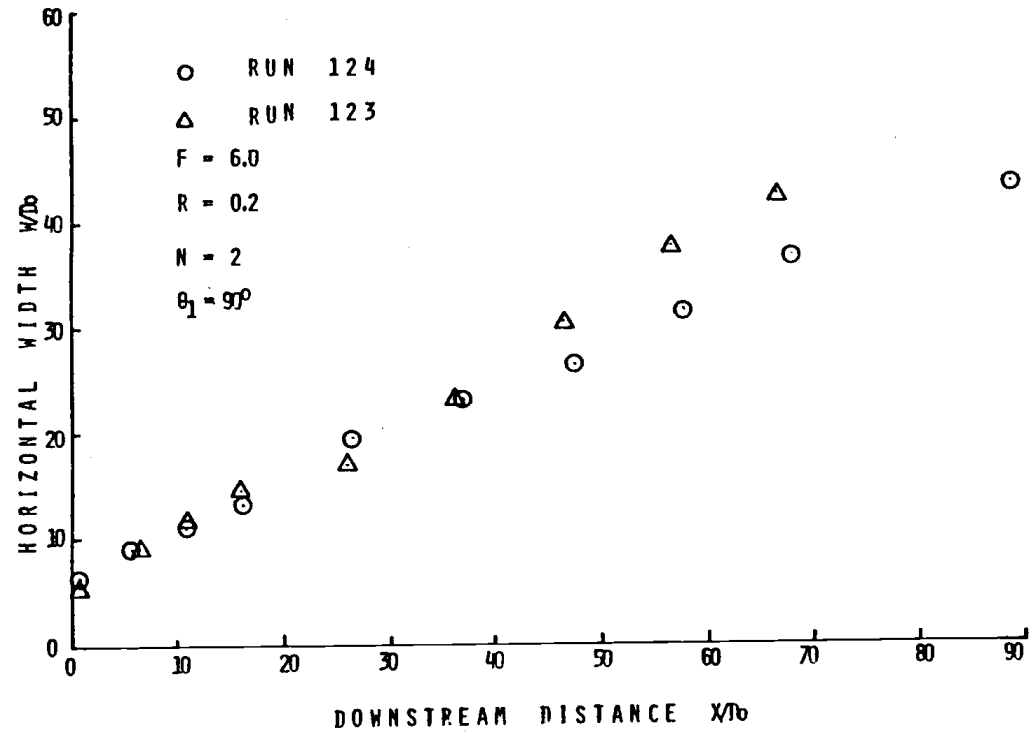

FIGURE 16: Horizontal Width for F=6.0, R=0.2, θ_1=90°, N=2

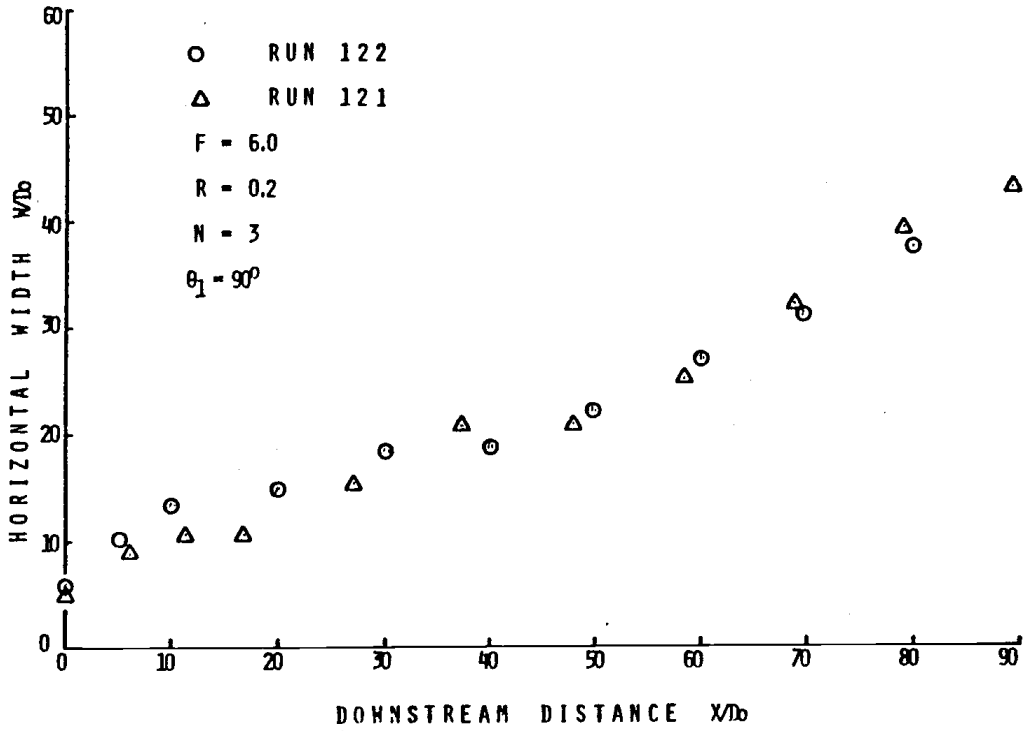

FIGURE 17: Horizontal Width for F=6.0, R=0.2, $\theta_1=90^{o}$, N=3

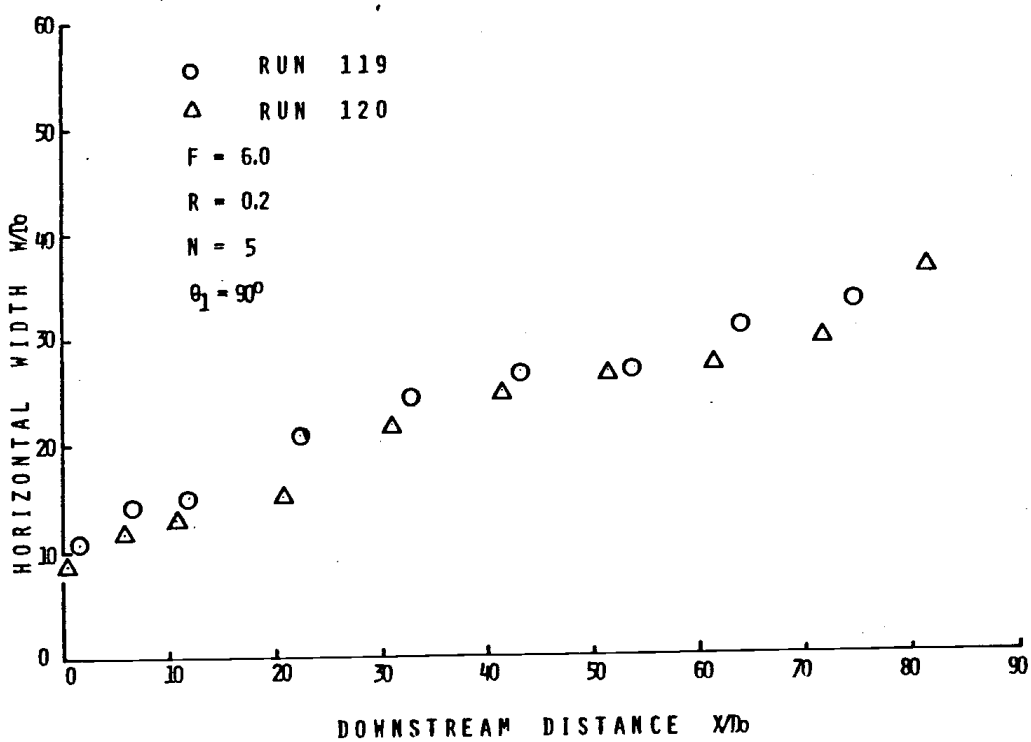

FIGURE 18: Horizontal Width for F=6.0, R=0.2, $\theta_1=90^{o}$, N=5

scattered much more than Z_{max} data. Though scattered they show linear dependence on x/D.

Normalized area A w/($N \frac{\Pi}{4} D_o^2$) (Figures 11 and 12) for (N = 7, $\theta_1 = 90^o$, L/D = 1.33) shows again linear dependence between the area and downstream distance.

Normalized area increases with lower velocity ratio. This area is a measure of dilution.

4.3 Effects of Number of Ports

The upper edge trajectories (Figures 13 and 14) of buoyant merging jets for constant velocity ratio R = 0.2 and $\theta_1 = 90^o$, L/D = 1.33 shows vertical discharge rapidly bending into a straight line for N = 7 and 5. For N = 3, 2 and 1 the curves keep bending in the crossflow.

Horizontal width $\frac{W}{D_o}$ (Figures 11, 12-17) for R = 0.2, $\theta_1 = 90^o$, L/D = 1.33) shows little effect of number of ports on the angle of plume spreading. Lines for N = 7 and 5 are straight. In the case of N = 2, the two jets interfere with each other in such a manner that they spread in the horizontal direction much faster than in the vertical (Plate 13 and 14).

Normalized area A x/($N \frac{\Pi}{9} D_o^2$) (Figures 17 and 18) for (R = 0.2, $\theta = 90^o$, L/D = 1.33) shows linear increase with downstream distance for N = 7 and 5. For N = 1 and 2 increase is curved upward. From Figure 5 one can see how the normalized area in the case of merging

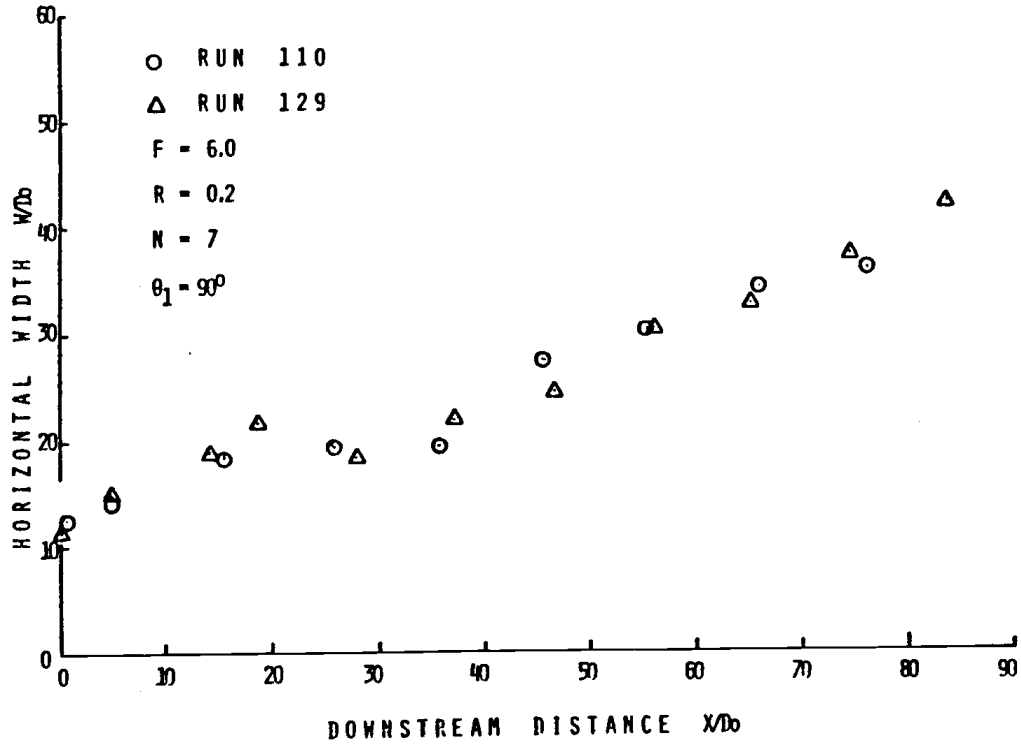

FIGURE 19: Horizontal Width for F=6.0, R=0.2, θ_1=90°, N=7

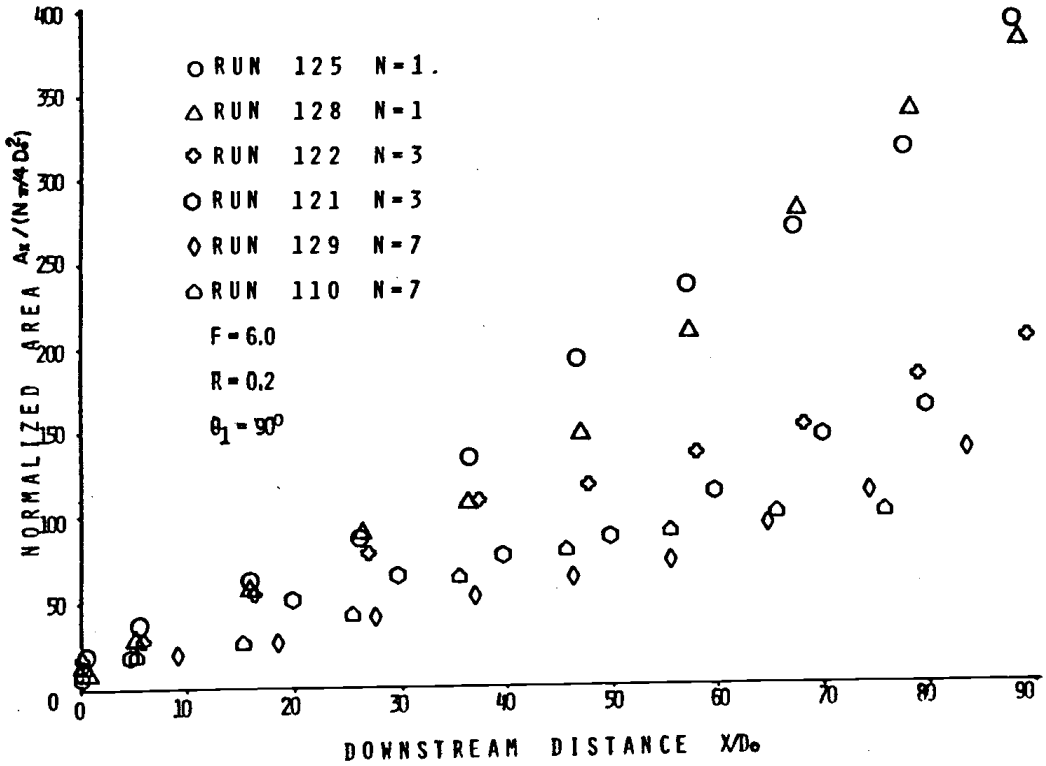

FIGURE 20: Effect of N on Normalized Area for F=6.0, R=0.2, θ_1=90°, N=1,3,7

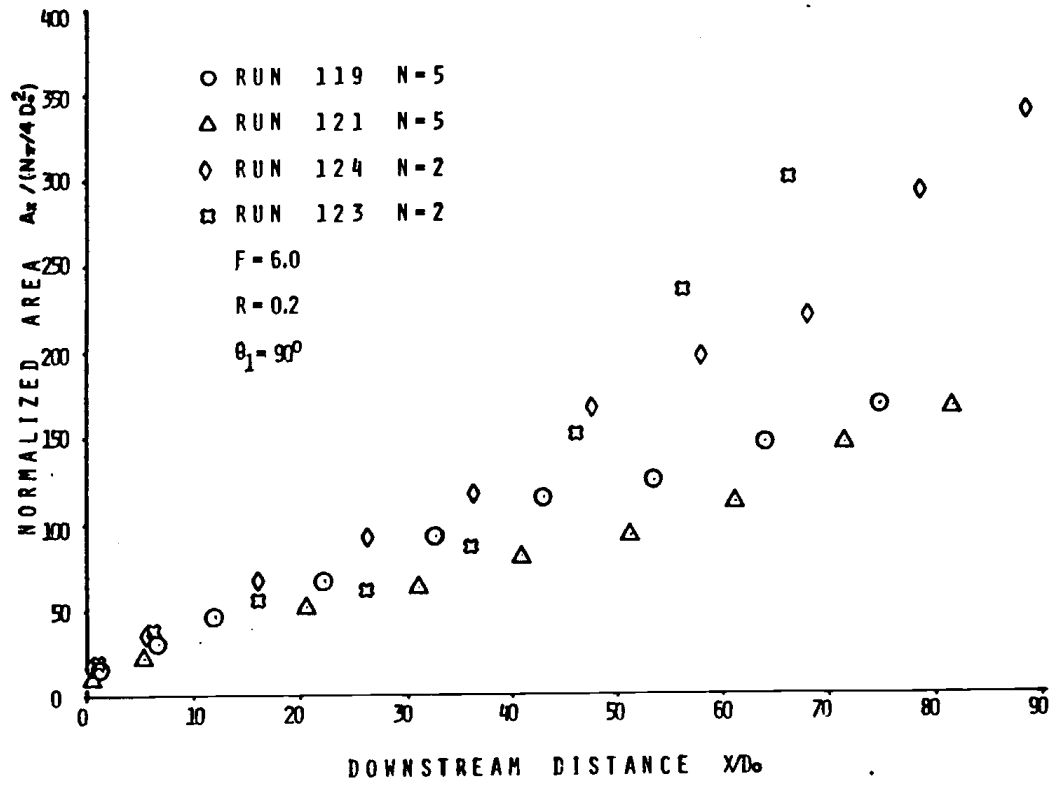

FIGURE 21: Effect of N on Normalized Area for F=6.0, R=0.2, θ_1=90°, N=2,5

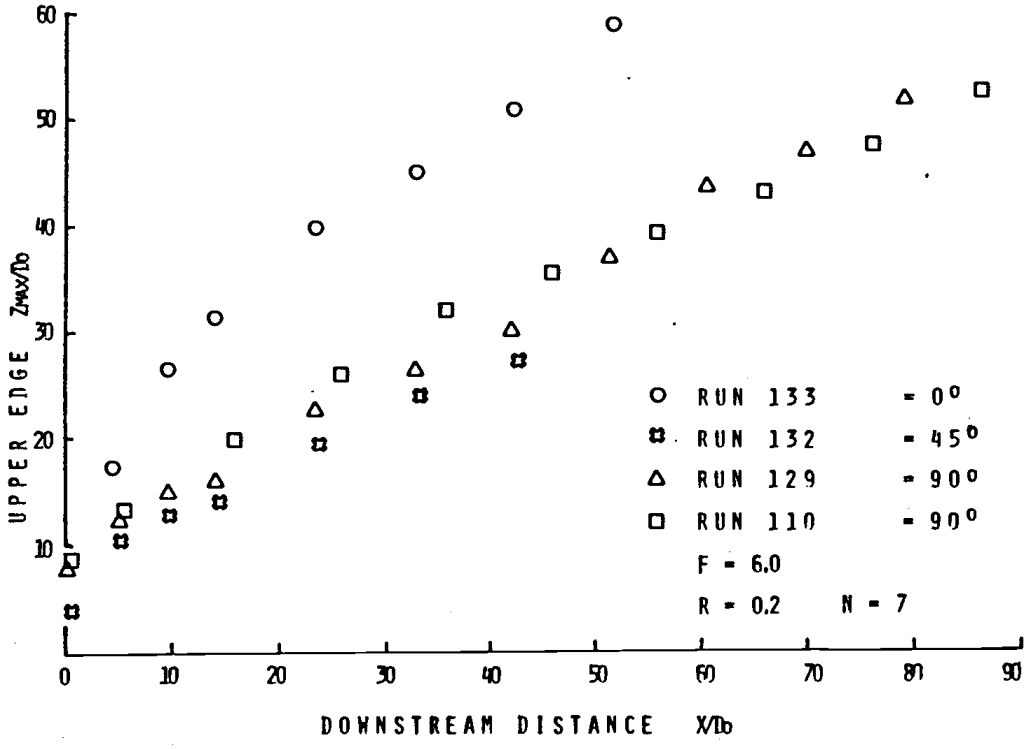

FIGURE 22: Effect of θ_1 on Upper Edge Trajectory for F=6.0, N=7, R=0.2

shrinks rapidly. When discharging from single port, entrainment of ambient fluid is the highest. Cross section of a single jet enlarged from 1 at the port exit to ≃ 400 at X/D_o = 90, compared to 130 for N = 7. If we can in a first approximation assume that velocities inside the jet at X/D_o = 90 are only slightly different from ambient velocity and that concentrations inside the instantaneous cross-section are uniform (pictures indicate this, all the boundaries are sharp and do not asimtotically merge into the ambient). Than normalized area gives us a measure of dilution.

4.4 Effect of the angle between crossflow and line connecting ports.

Shape of the cross section changes drastically for different angles.

When θ_1 = 0° (i.e., crossflow parallel to nozzle line) twin vortex structure is formed rapidly. (Plate). When θ_o^o = 45, the jets are rolled in space like a band (Plate 133) along with x axis. When θ_1 = 90° neither of these effects dominated. Twin vortex was observed only at the lowest towing velocity at R = 0.1 (Plate 117a and 131).

Upper edge trajectory is the highest for θ_1 = 0 where the jets cut thru the ambient fluid. The lowest is for θ_1 = 45° where the jets are rolled.

The normalized area is the highest for θ_1 = 0, where entrainment is propelled additionally by huge vortex pair.

At θ_1 = 45° the normalized area is the smallest.

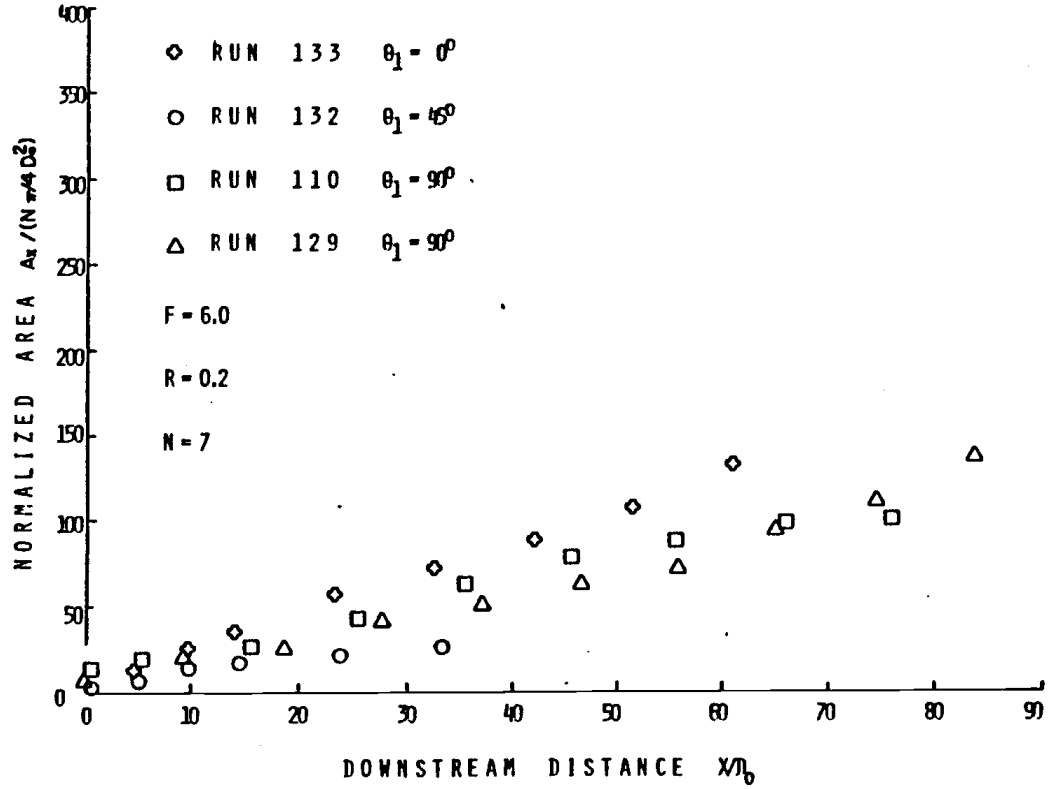

FIGURE 23: Effect of θ_1 on Normalized Area for F=6.0, N=7, R=0.2

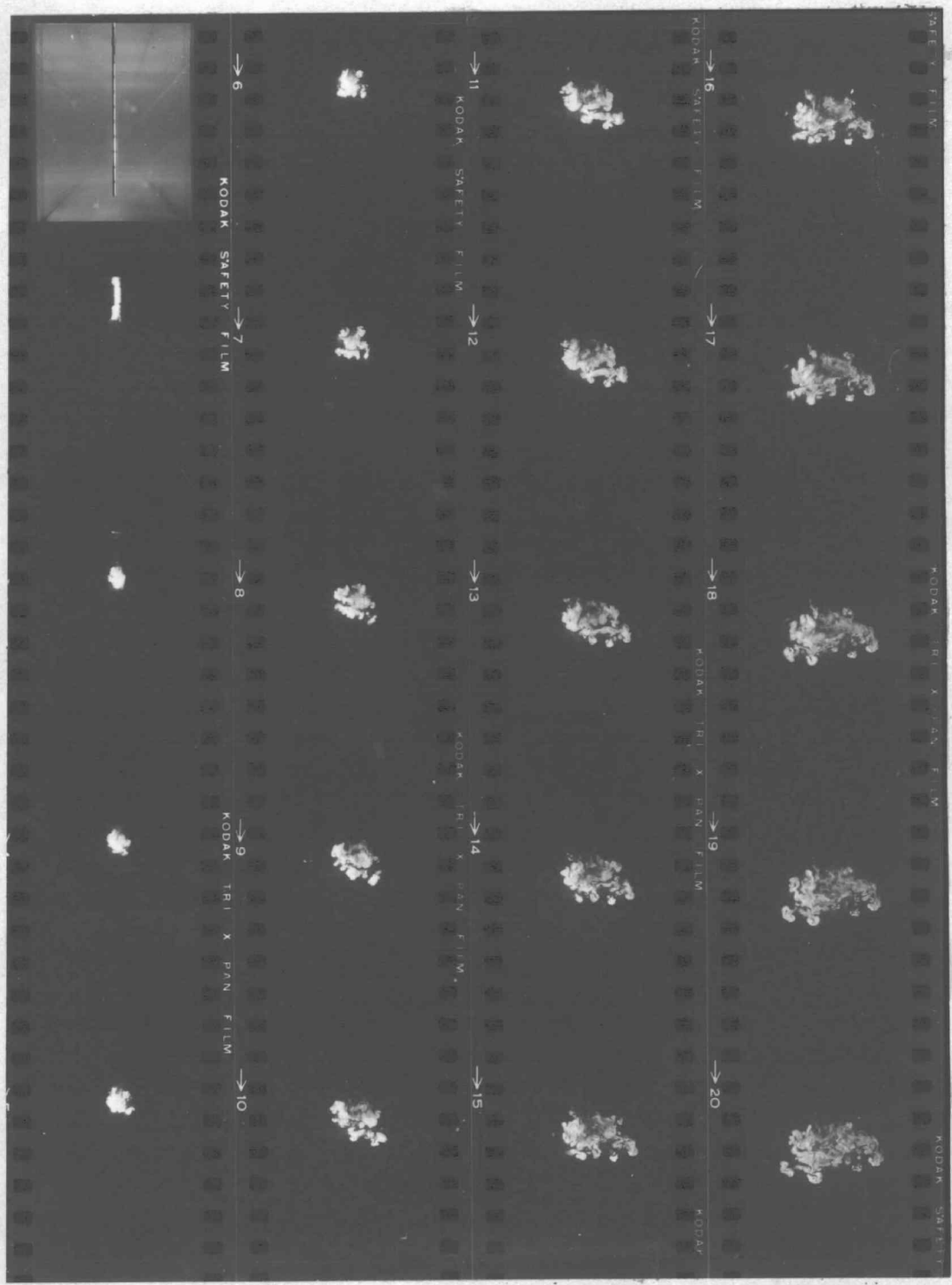

$F = 6.0$ $N = 1$ $\theta_1 = 90°$ $R = 0.2$

$\frac{x}{x_0} = 0.5$ $\Delta X/D_0 = 5.2$ EXPOSURE LENGTH = 1.46

PLATE 15 : Cross-sections through buoyant jet for Run 125

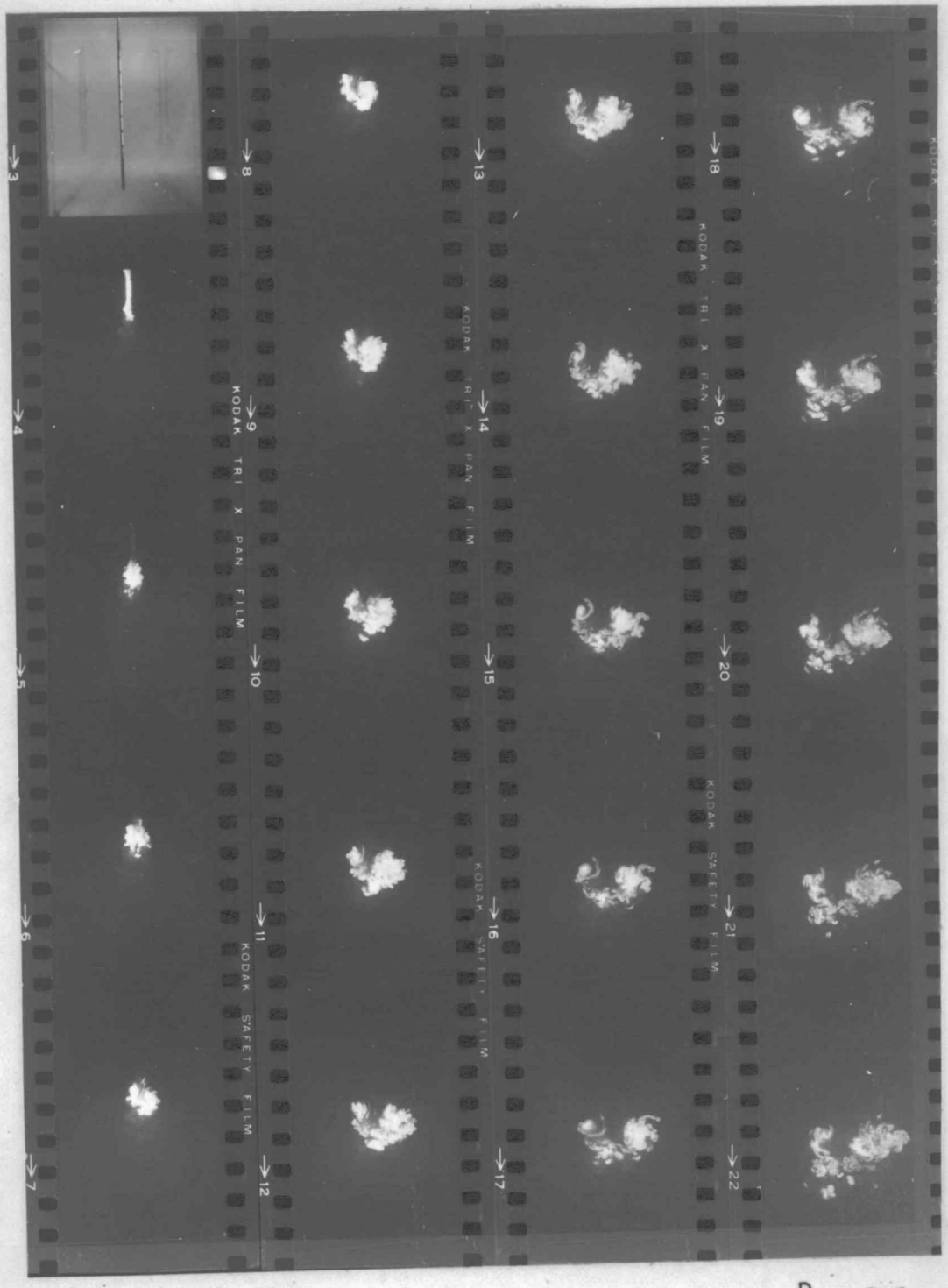

F = 6.0 N = 1 R = 0.1

$\frac{v}{v_0}$ = 0.0 $\Delta X/D_0$ = 2.6 EXPOSURE LENGTH = 0.73

PLATE 16 ; Cross-sections through buoyant jet for Run 127

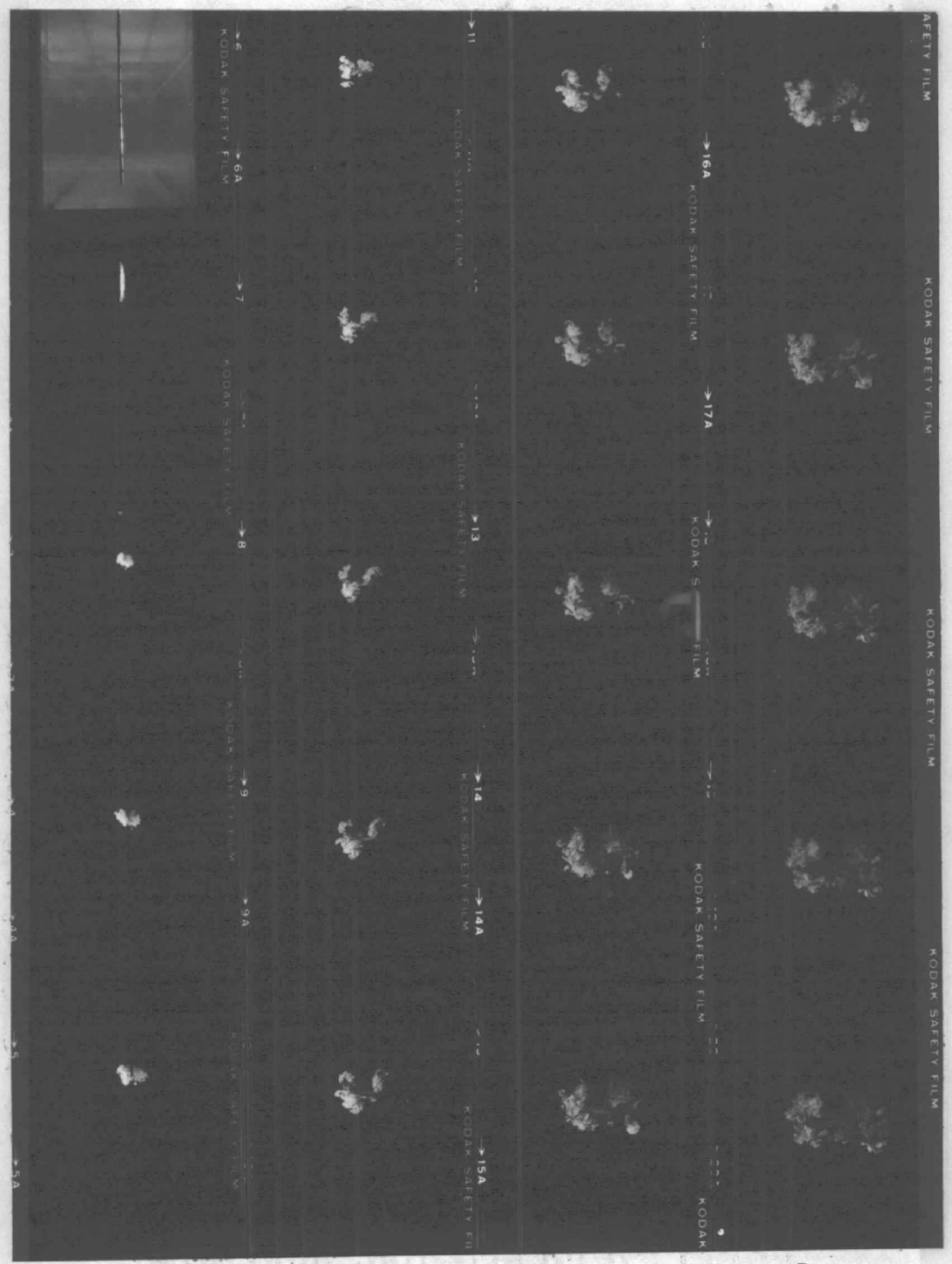

F = 6.0 N = 1 R = 0.2

X_0 = 0.5 $\Delta X/D_0$ = 5.2 EXPOSURE LENGTH = 1.5

PLATE 17 : Cross-sections through buoyant jet for Run 128

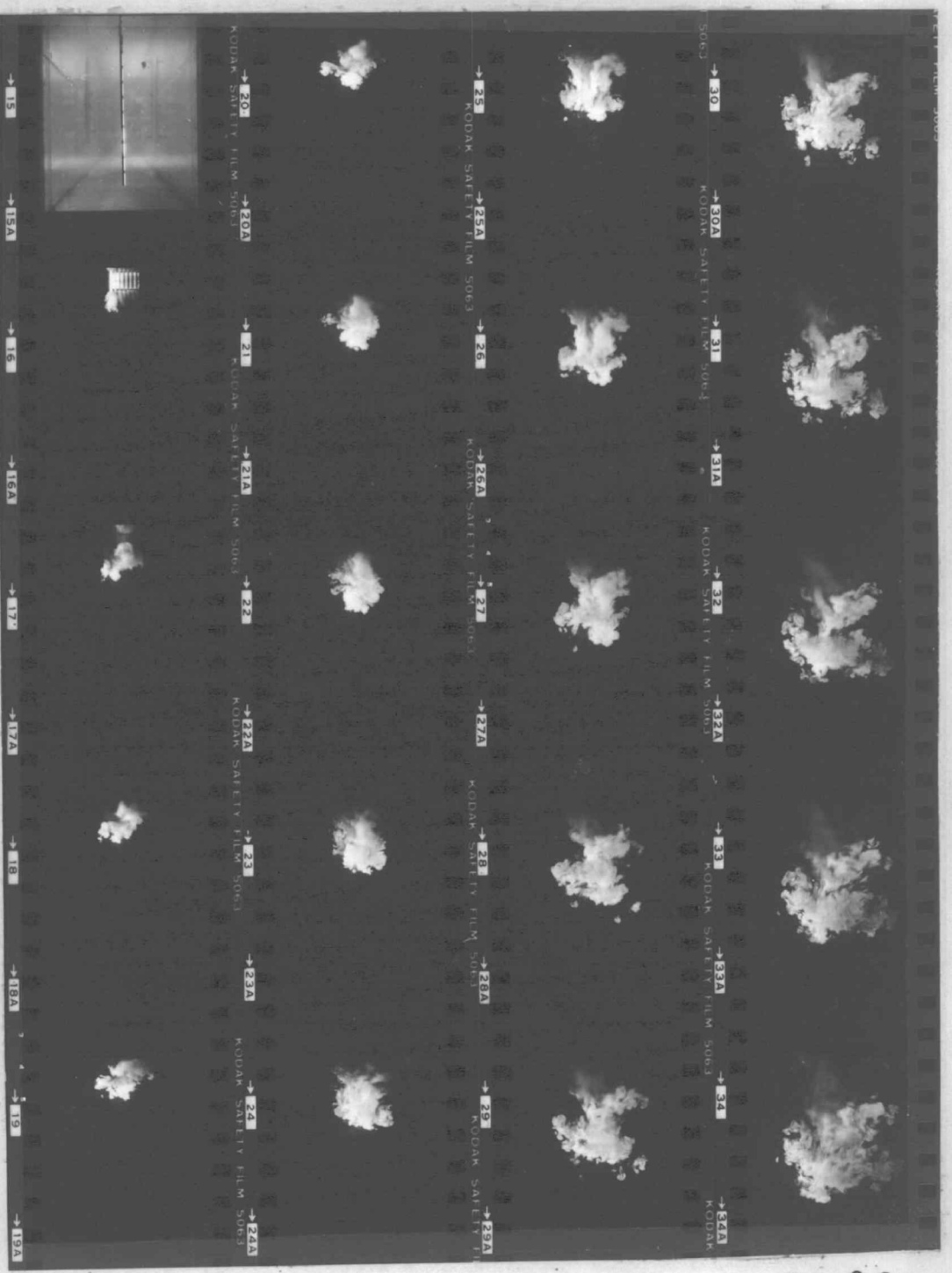

$F = 6.0$ $N = 7$ $\theta_1 = 90°$ $R = 0.2$

$\frac{x}{x_0} = 0.0$ $\Delta X/D_0 = 4.7$ EXPOSURE LENGTH = 1.45

PLATE 18 : Cross-sections through buoyant jet for Run 129

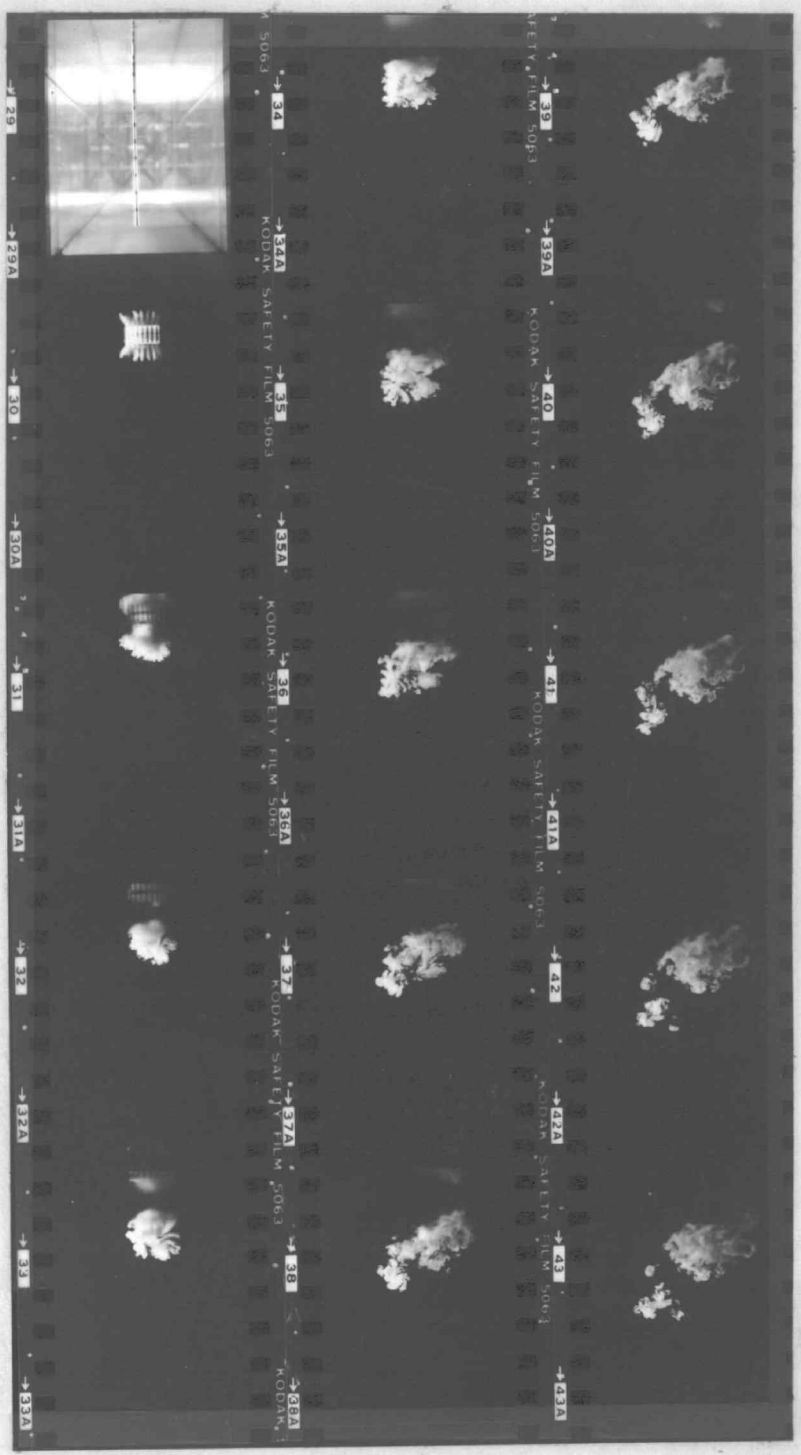

$F = 6.0$ $N = 7$ $\theta_1 = 90°$ $R = 0.5$

$X/D_0 = 0.0$ $\Delta X/D_0 = 12.0$ EXPOSURE LENGTH = 3.75

PLATE 19 : Cross-sections through buoyant jet for Run 130

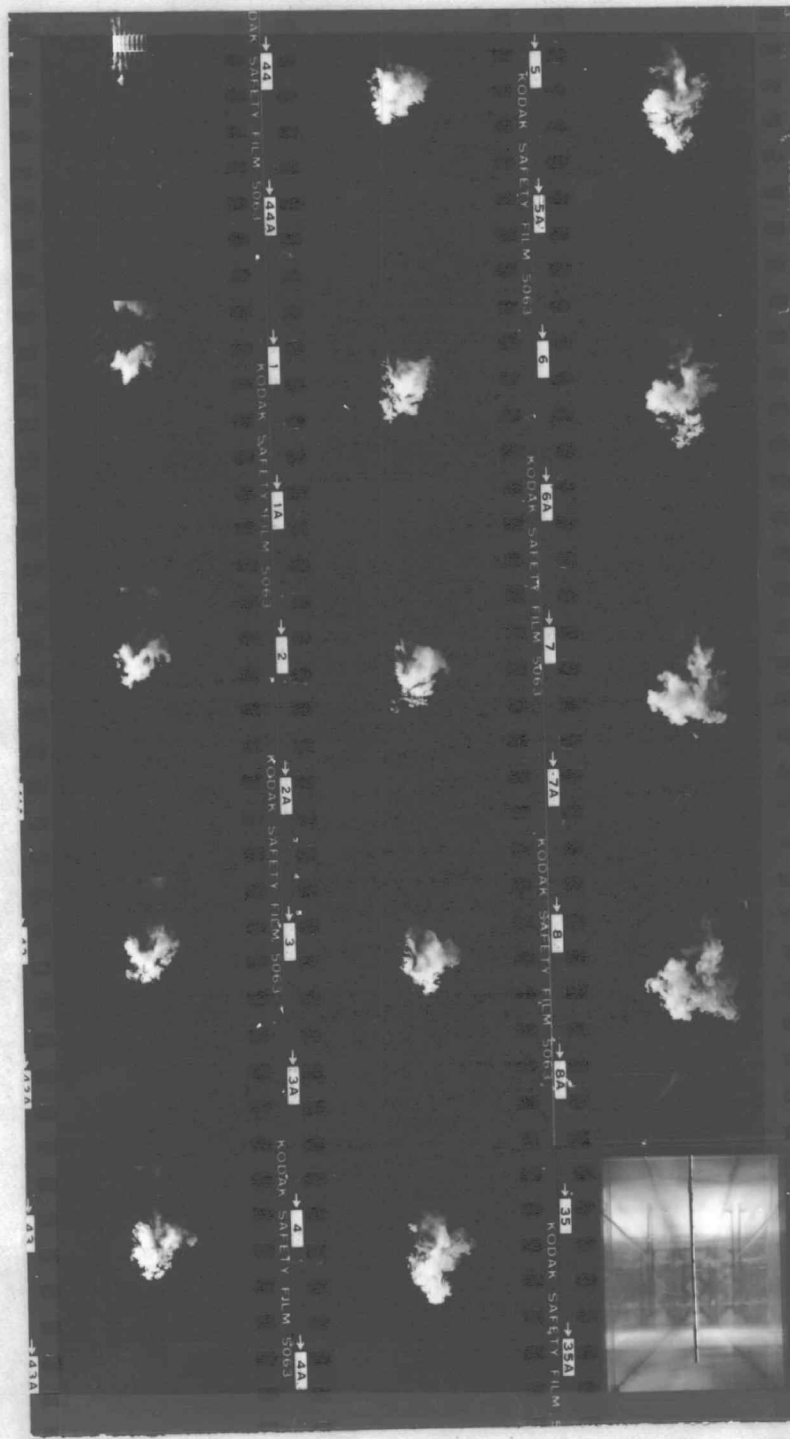

F = 6.0 N = 7 θ_1 = 90° R = 0.1

$\frac{Y}{D_0}$ = -0.5 $\Delta X/D_0$ = 2.3 EXPOSURE LENGTH = 0.71

PLATE 20 : Cross-sections through buoyant jet for Run 131

F = 6.0 N = 7 $\theta_1 = 0°$ R = 0.2

$\frac{y}{\lambda_0} = 0.0$ $\Delta X/D_0 = 4.68$ EXPOSURE LENGTH = 1.46

PLATE 21 : Cross-sections through buoyant jet for Run 133

V. CONCLUSIONS

This investigation dealt with merging buoyant jets from a finite number of ports placed in a line, subject to crossflow from different angles. The visualization technique used was somewhat unusual in this field. A plane light beam and motor-driven camera produced three dimensional picture composed of vertical cross-sections thru the plume in equal intervals downstream. The picture gave the size and position of the instantaneous cross-section which was averaged out slightly by the finite dimension of the plane light beam and exposure length of the illuminated portion of the plume for a particular ambient velocity. Experimental parameters were chosen so that the effects of the velocity ratio R, number of ports N and angle of crossflow with respect to the nozzle line θ_1 were investigated.

Buoyant merging jets were strongly influenced by the velocity ratio. At fixed N and θ_1, upper edge trajectories, plume widths and normalized areas appeared to increase linearly (from w = 10 D on). The normalized area increases with lower velocity ratio.

At fixed R and θ_1, upper edge trajectories, horizontal widths and normalized areas appear to increase linearly downstream for N = 7 and 5. Trajectories are lower for smaller N. For a single jet twin vortices were observed. Normalized area reduces rapidly with increasing N, showing reduced entrainment when two or more jets compete for the same fluid.

At fixed N and R orientation of the nozzles θ_1 changes drastically the shape of cross-section. At $\theta_1 = 0^o$, the vortex pair is very strong and it aids entraining ambient fluid, so normalized area is the highest. At $\theta = 45^o$ jets are rolled in space like a band. At 90^o vortex appears only at lowest velocity ratio, R = 0.1.

Hopefully the data presented in this investigation will be of some help to all those who model merging buoyant plumes in a crossflow analytically.

LIST OF REFERENCES

1. Pai, S. I. Fluid Dynamics of Jets, D. Van Nostrand Co., 1954.

2. Abramovich, G. N. The Theory of Turbulent Jets, M.I.T. Press, (translation), Cambridge, Massachusetts, 1963.

3. Rajaratnam , N. Turbulent Jets, Elsevier, 1976.

4. Davis, L. R., and M. A. Shirazi: A Review of Thermal Plume Modelling. Keynote Address, Proceedings of the Sixth International Heat Transfer Conference, Toronty, Canada, August, 1978.

5. Hirst, E. A. Analysis of Round, Turbulent, Buoyant Jets Discharged to Flowing Stratified Ambients. Oak Ridge National Laboratory, Report ORNL 4685, June, 1971.

6. Wright, S. J. Effects of Ambient Crossflow and Density Stratification on the Characteristic Behavior of Round Turbulent Buoyant Jets. Ph.D. Thesis, California Institute of Technology, Pasadina, California, 1977.

7. Jirka, G. and D. R. F. Harleman. The mechanics of Submerged Multiport Diffusers for Buoyant Discharges in Shallow Water, M.I.T., R. M. Parsons Lab., Report 167, March, 1973.

8. Kannberg, L. D. and L. R. Davis. An Analysis of Deep Submerged Multiple Port Buoyant Discharges
Transactions of ASME J. of Heat Transfer, Vol. 99, p. 698-655, Nov. 1977.

9. Macduff, R. B. and L. R. Davis. "Multiple Cell Mechanical Draft Cooling Tower Model" in ASME symposium volume Environmental Effects of Atmosphere Heat/Moisture Releases. Palo Alto, California, May, 1978.

10. Kannberg, L. D. An Experimental and Analytical investigation of deep submerged multiple buoyant jets. Ph.D. Thesis, Oregon State University, Corvallis, Oregon, 1976.

11. Davis, L. R., M. A. Shirazi, and D. L. Slegel. Experimental simulation of single and multiple cell cooling tower plumes. Corvallis Environmental Research Laboratory, U.S.E.P.A., Corvallis, 1976.

12. Bradshaw, P. Experimental Fluid Mechanics, Pergamon Press, 2nd Edition, 1970.

13. Merzkirch, W. Flow Visualization, Academic Press, 1974.

14. Werle, H. Hydrodynamic Flow Visualization, Annual Review in Fluid Mechanics, pp. 361-82, 1973.

15. Clayton, B. R. and B. S. Massey. Flow Visualization in Water: A Review of Techniques. J. Sci. Instrum., 44, pp. 2-11, 1967.

16. Benedict, B. A., J. L. Anderson and E. L. Yandell, Jr. Analytical Modeling of Thermal Discharges. A Review of the State-of-the-Art. Argonne National Laboratories. ANL/ES-18, April 1974.

17. Fan, Loh-Nien. Turbulent Buoyant Jets into Stratified or Flowing Ambient Fluids. W. M. Keck Laboratory of Hydraulics and Water Resources, California Institute of Technology, Report No. KH-R-15, June 1967.

APPENDIX

RUN 112

FRAME	TIME	X/Do	Zmax/Do	Zmin/Do	Zc/Do	B	W	AREA
8	0.00	7.0	5.2	-2.6	1.3	7.8	14.3	15.18
9	0.86	32.1	4.5	-2.6	1.0	7.1	11.4	10.10
10	1.71	57.2	7.7	-2.6	2.6	10.3	16.0	20.24
11	2.57	82.3	10.0	-2.6	3.7	12.6	18.6	26.7
12	3.43	107.4	12.4	-2.6	4.9	15.0	22.3	32.2

RUN 130

FRAME	TIME	X/Do	Zmax/Do	Zmin/Do	Zc/Do	B	W	AREA
30	0.0	0.0	5.0	0.0	2.5	5.0	12.2	6.9
31	0.8	12.0	8.5	-2.6	3.0	10.1	15.1	18.4
33	2.4	36.0	14.8	-0.5	7.2	15.3	15.6	28.5
35	4.0	60.0	18.3	0.8	9.6	17.5	20.0	38.2
37	5.6	84.0	22.5	0.8	11.7	21.7	22.0	48.3
39	7.2	108.0	27.0	1.0	14.0	26.0	29.7	53.8

TABLE 2: Tabulated data reduced from pictures.